

**Color Dipole Picture of Deep Inelastic Scattering,
Revisited.**

Masaaki Kuroda

Center for Liberal Arts, Meijigakuin University
Yokohama, Japan

Dieter Schildknecht

Fakultät für Physik, Universität Bielefeld
D-33501 Bielefeld, Germany
and

Max-Planck Institut für Physik (Werner-Heisenberg-Institut),
Föhringer Ring 6, D-80805, München, Germany

Abstract

Based upon the color-dipole picture, we provide closed analytic expressions for the longitudinal and the transverse photoabsorption cross sections at low values of the Bjorken variable of $x \lesssim 0.1$. We compare with the experimental data for the longitudinal-to-transverse ratio of the (virtual) photoabsorption cross section and with our previous fit to the experimental data for the total photoabsorption cross section. Scaling in terms of the low-x scaling variable $\eta(W^2, Q^2)$ is analyzed in terms of the reduced cross section of deep inelastic scattering.

1 Introduction

The process of deep inelastic scattering (DIS) at low values of the Bjorken variable, $x \cong Q^2/W^2 \lesssim 0.1$, where $Q^2 \geq 0$ and W^2 refer to the virtuality of the photon and the photon-nucleon center of mass energy squared, is determined by the virtual dissociation of the photon into hadronic vector states that subsequently interact with the nucleon (generalized vector dominance (GVD)) [1], [2], [3]. In QCD, the hadronic vector states are quark-antiquark states that interact as color dipoles with the gluon field in the nucleon by exchange of (at least) two gluons that form a color-neutral state (color dipole picture (CDP)) [4], [5], [6], [7], [8]. The color-gauge invariant interaction with the gluon field in the nucleon – without specific parameterization of this interaction [9] – implies color transparency and saturation,¹ respectively dependent on the relative magnitude of Q^2 and W^2 within the region of $x \lesssim 0.1$.

The quantitative analysis of the experimental data on the photon absorption cross section, or, equivalently, the proton structure functions, requires a fit [7], [8] [9] to the experimental data on DIS based on the small number of two to four free parameters, the number of parameters dependent on which ones are considered to be fixed by theoretical considerations.

In Section 2, we present concise and simple closed analytic expressions for the longitudinal and transverse photoabsorption cross sections. In Section 3, our results are summarized in a convenient form to be used in elaborate fits by experimentalists to the body of experimental data. We compare our theoretical predictions for the total photoabsorption cross section and the longitudinal-to-transverse ratio with experimental data. Some conclusions will be drawn in Section 4. Technical details are given in Appendices A to C.

2 The Photoabsorption Cross Section in the Color Dipole Picture, Theory

In Section 2.1, we summarize the essential results from the color dipole picture (CDP). In Section 2.2 various refinements will be presented.

¹Compare also the recent reviews in ref. [10]

2.1 The color dipole picture, formulation from 2000.

The approach of the color dipole picture (CDP) to deep inelastic scattering² at low $x \cong Q^2/W^2 \lesssim 0.1$ may be summarized by the photoabsorption cross section [6], [5],

$$\sigma_{\gamma_{L,T}^*}(W^2, Q^2) = \int dz \int d^2\vec{r}_\perp \left| \psi_{L,T}(\vec{r}_\perp, z(1-z), Q^2) \right|^2 \sigma_{(q\bar{q})p}(\vec{r}_\perp, z(1-z), W^2), \quad (2.1)$$

supplemented by the representation of the dipole cross section,

$$\sigma_{(q\bar{q})p}(\vec{r}_\perp, z(1-z), W^2) = \int d^2\vec{l}_\perp \tilde{\sigma}(\vec{l}_\perp^2, z(1-z), W^2) (1 - e^{-i\vec{l}_\perp \vec{r}_\perp}) \quad (2.2)$$

that guarantees the gauge-invariant interaction of the quark-antiquark ($q\bar{q}$) color dipole with the gluon field in the proton via two-gluon coupling. The “photon wave function” squared, $|\psi_{L,T}(\vec{r}_\perp, z(1-z), Q^2)|^2$, in (2.1) is determined by QED. It gives the probability for the fluctuation of the (virtual) photon of virtuality $Q^2 \geq 0$ into a $q\bar{q}$ dipole state of configuration $(\vec{r}_\perp, z(1-z))$. The variable \vec{r}_\perp in (2.1) and (2.2) determines the transverse $q\bar{q}$ -separation variable of the $q\bar{q}$ state, and $0 \leq z \leq 1$ characterizes the longitudinal momentum partition between quark and antiquark in that state.

The right-hand side in (2.1) contains the (required) factorization of the Q^2 -dependent photon wave function and the W -dependent dipole cross section: the photon of virtuality $q^2 = -Q^2 \leq 0$ virtually dissociates (GVD [1], [2], [3]), or fluctuates in modern jargon, into $q\bar{q}$ states of masses³ $M_{q\bar{q}} > 0$ that propagate and interact with the proton at the center-of-mass energy W . In ref. [6] the formulation of (2.1) with (2.2) of the CDP was explicitly derived from GVD supplemented by the QCD-based color-dipole structure of the interacting $q\bar{q}$ vector states. The dependence on W of the dipole cross section in (2.1) is a strict consequence from the mass dispersion-relation (compare Appendix B) of GVD; the necessary dependence on W in (2.1) (rather than a dependence on $x \cong Q^2/W^2$ [5]), using functional methods of quantum field theory, was more recently elaborated upon in great detail in ref. [13].

The representation of the photoabsorption cross section (2.1), in conjunction with the color-gauge-invariant representation of the $q\bar{q}$ -dipole-proton interaction (2.2), implies

²Compare ref. [11] for the application of the CDP to deeply virtual Compton scattering and vector meson production, and ref. [12] for the treatment of ultra-high-energy neutrino-nucleon scattering.

³The appropriate Fourier transform introduces the transverse $q\bar{q}$ -separation variable \vec{r}_\perp and the longitudinal momentum partition, z .

the essential qualitative feature of the experimental results: the scaling of the total photoabsorption cross section $\sigma_{\gamma^*p}(W^2, Q^2) = \sigma_{\gamma^*p}(\eta(W^2, Q^2))$ in the low-x scaling variable $\eta(W^2, Q^2)$ [7], [8], [9], see (2.5) below, as $1/\eta(W^2, Q^2)$ for $\eta(W^2, Q^2) \gg 1$, (“color transparency”) and as $\ln(1/\eta(W^2, Q^2))$ for $\eta(W^2, Q^2) \ll 1$ (“saturation”). As elaborated upon in detail in ref. [9], no parameter-dependent explicit ansatz for the dipole cross section (2.2) is required to arrive at this general conclusion.

For an explicit quantitative description of the experimental results on the total photoabsorption cross sections for longitudinally and transversely polarized photons, a parameter-dependent specification of the dipole cross section is required. In ref. [7], the general expression for the photoabsorption cross section in (2.1) with (2.2) is supplemented by the ansatz

$$\tilde{\sigma}(\vec{l}_\perp^2, z(1-z), W^2) = \frac{\sigma^{(\infty)}(W^2)}{\pi} \delta(\vec{l}_\perp^2 - z(1-z)\Lambda_{sat}^2(W^2)) \quad (2.3)$$

that implies

$$\sigma_{(q\bar{q})p}(\vec{r}_\perp, z(1-z), W^2) = \sigma^{(\infty)}(W^2) \left(1 - J_0(r_\perp \sqrt{z(1-z)\Lambda_{sat}(W^2)})\right). \quad (2.4)$$

In (2.3) and (2.4), $\sigma^{(\infty)}(W^2)$ denotes a weakly (logarithmically) on W^2 dependent cross section of hadronic magnitude to be elaborated upon later, \vec{l}_\perp denotes the transverse part of the three-momentum of the gluon absorbed by the $q\bar{q}$ dipole state, and $\Lambda_{sat}^2(W^2)$ denotes the “saturation scale” that increases with a small power of W^2 . The ansatz (2.3) implies, and is motivated by, a required increase of the effective transverse momentum of the absorbed gluon with increasing energy W . The function $J_0(r_\perp \sqrt{z(1-z)\Lambda_{sat}(W^2)})$ in (2.4) is the zero-order Bessel function.

We also note the low-x scaling variable, $\eta(W^2, Q^2)$, given by [7]

$$\eta(W^2, Q^2) = \frac{Q^2 + m_0^2}{\Lambda_{sat}^2(W^2)}. \quad (2.5)$$

In addition to (2.5), it is useful to introduce the ratio

$$\mu(W^2) = \frac{m_0^2}{\Lambda_{sat}^2(W^2)}. \quad (2.6)$$

The low-x scaling variable $\eta(W^2, Q^2)$ becomes $\eta(W^2, Q^2) = Q^2/\Lambda_{sat}^2(W^2) + \mu(W^2) \geq \mu(W^2)$. The mass m_0 in (2.5) and (2.6) denotes the effective onset of hadron production in

e^+e^- annihilation to hadrons, and, from quark-hadron duality [14], we have $0 < m_0^2 < m_\rho^2$, where m_ρ denotes the ρ -meson mass.⁴

The evaluation of the photoabsorption cross section (2.1), upon insertion of (2.4), leads to [7]

$$\sigma_{\gamma_{L,T}^* p}(W^2, Q^2) = \frac{\alpha R_{e^+e^-}}{3\pi} \sigma^{(\infty)}(W^2) I_{L,T}(\eta(W^2, Q^2), \mu(W^2)). \quad (2.7)$$

In (2.7), $R_{e^+e^-} = 3 \sum_q Q_q^2$, where the sum runs over the actively contributing quark flavors, and Q_q denotes the quark charge.

It turns out that the relevant region of $\mu(W^2)$ fulfills the bound $\mu(W^2) < 1$. Under this assumption $I_{L,T}(\eta(W^2, Q^2), \mu(W^2))$ becomes [7]

$$I_{L,T}(\eta(W^2, Q^2), \mu(W^2)) = I_{L,T}^{(1)}(\eta(W^2, Q^2), \mu(W^2)) (1 + 0(\mu(W^2))), \quad (2.8)$$

where $I_L^{(1)}(\eta(W^2, Q^2), \mu(W^2))$ and $I_T^{(1)}(\eta(W^2, Q^2), \mu(W^2))$ are given by

$$\begin{aligned} I_L^{(1)}(\eta, \mu) &= \frac{\eta - \mu}{\eta} \\ &\times \left(1 - \frac{\eta}{\sqrt{1 + 4(\eta - \mu)}} \ln \frac{\eta(1 + \sqrt{1 + 4(\eta - \mu)})}{4\mu - 1 - 3\eta + \sqrt{(1 + 4(\eta - \mu))((1 + \eta)^2 - 4\mu)}} \right), \\ I_T^{(1)}(\eta, \mu) &= \frac{1}{2} \ln \frac{\eta - 1 + \sqrt{(1 + \eta)^2 - 4\mu}}{2\eta} - \frac{\eta - \mu}{\eta} + \frac{1 + 2(\eta - \mu)}{2\sqrt{1 + 4(\eta - \mu)}} \\ &\times \ln \frac{\eta(1 + \sqrt{1 + 4(\eta - \mu)})}{4\mu - 1 - 3\eta + \sqrt{(1 + 4(\eta - \mu))((1 + \eta)^2 - 4\mu)}}. \end{aligned} \quad (2.9)$$

We note the photoproduction ($Q^2 = 0$) limit of (2.7) with (2.9). Inserting $\eta = c\mu(W^2)$ into (2.9), where $c = \text{const} \geq 1$ and $0 < \mu(W^2) < 1$, a careful evaluation of the photoproduction limit of $c \rightarrow 1$ leads to

$$\begin{aligned} \lim_{\eta \rightarrow \mu} \sigma_{\gamma_{L,T}^* p}(W^2, Q^2) &= 0, \\ \sigma_{\gamma p}(W^2) &\equiv \lim_{\eta \rightarrow \mu} \sigma_{\gamma_{T,p}^*}(W^2, Q^2) = \frac{\alpha R_{e^+e^-}}{3\pi} \sigma^{(\infty)}(W^2) \ln \frac{1}{\mu}. \end{aligned} \quad (2.10)$$

In the limit of very high energy, $\mu(W^2) \ll 1$, (2.9) may be further simplified. We note that $\mu(W^2) \leq \eta(W^2, Q^2) \leq \eta_{Max}(W^2)$, where $\eta_{Max}(W^2)$ is determined by the required

⁴For heavy flavors, like charm, the mass scale m_0^2 must be appropriately modified.

restriction to low values of $x \leq x_0 \lesssim 0.1$, or $Q^2 \leq x_0 W^2$, i.e.

$$\eta(W^2, Q^2) \leq \eta_{Max}(W^2) = \frac{x_0 W^2}{\Lambda_{sat}^2(W^2)}. \quad (2.11)$$

With $\mu(W^2) \ll 1$ and $\eta(W^2, Q^2) \geq \mu(W^2)$, upon making use of the identity

$$\begin{aligned} 2 \ln \frac{\sqrt{1+4\eta} + 1}{\sqrt{1+4\eta} - 1} &= \ln \frac{(1+\eta)\sqrt{1+4\eta} + 1 + 3\eta}{\eta(\sqrt{1+4\eta} - 1)} = \\ &= \ln \frac{\eta(1 + \sqrt{1+4\eta})}{(1+\eta)\sqrt{1+4\eta} - 1 - 3\eta}, \end{aligned} \quad (2.12)$$

and of the definition

$$I_0(\eta) = \frac{1}{\sqrt{1+4\eta}} \ln \frac{\sqrt{1+4\eta} + 1}{\sqrt{1+4\eta} - 1}, \quad (2.13)$$

we find that (2.9) becomes

$$\begin{aligned} I_L^{(1)}(\eta, \mu) &= \frac{\eta - \mu}{\eta} (1 - 2\eta I_0(\eta)), \\ I_T^{(1)}(\eta, \mu) &= I_0(\eta) - \frac{\eta - \mu}{\eta} (1 - 2\eta I_0(\eta)), \end{aligned} \quad (2.14)$$

and, accordingly,

$$I_L^{(1)}(\eta, \mu) + I_T^{(1)}(\eta, \mu) = I_0(\eta). \quad (2.15)$$

With (2.14), (2.15) and (2.8), the longitudinal and the transverse parts of the photoabsorption cross section (2.7), and the total cross section

$$\sigma_{\gamma^*p}(W^2, Q^2) = \sigma_{\gamma_L^*p}(W^2, Q^2) + \sigma_{\gamma_T^*p}(W^2, Q^2), \quad (2.16)$$

explicitly become,

$$\begin{aligned} \sigma_{\gamma_L^*p}(W^2, Q^2) &= \frac{\alpha R_{e^+e^-}}{3\pi} \sigma^{(\infty)}(W^2) \frac{\eta - \mu}{\eta} (1 - 2\eta I_0(\eta)), \\ \sigma_{\gamma_T^*p}(W^2, Q^2) &= \frac{\alpha R_{e^+e^-}}{3\pi} \sigma^{(\infty)}(W^2) \left(I_0(\eta) - \frac{\eta - \mu}{\eta} (1 - 2\eta I_0(\eta)) \right), \\ \sigma_{\gamma^*p}(W^2, Q^2) &= \frac{\alpha R_{e^+e^-}}{3\pi} \sigma^{(\infty)}(W^2) I_0(\eta). \end{aligned} \quad (2.17)$$

Under the approximation of $\sigma^{(\infty)}(W^2) \cong \text{const}$ (actually $\sigma^{(\infty)}(W^2)$ varies as $\ln W^2$, see below), we have low-x scaling behavior [7],

$$\sigma_{\gamma^*p}(W^2, Q^2) = \sigma_{\gamma^*p}(\eta(W^2, Q^2)). \quad (2.18)$$

The longitudinal cross section in (2.17) vanishes in the $Q^2 = 0$ photoproduction limit of $\eta(W^2, Q^2) = \mu(W^2)$. For $\eta \gg \mu$, there is low-x scaling separately for the longitudinal and transverse parts of the cross section, $\sigma_{\gamma_{Lp}^*}(W^2, Q^2) = \sigma_{\gamma_{Lp}^*}(\eta(W^2, Q^2))$ and $\sigma_{\gamma_T^*}(W^2, Q^2) = \sigma_{\gamma_T^*}(\eta(W^2, Q^2))$.

It will be illuminating to examine the result (2.17) for different limits of η and μ .

- i) The limit of $\mu \ll 1$ combined with $\eta \gg 1$ (and $\eta \leq \eta_{Max}$). This limit corresponds to high energy W and relatively large photon virtualities, $Q^2 \gg \Lambda_{sat}^2(W^2)$. Employing the expansion,

$$\begin{aligned} I_0(\eta) &= \frac{2}{1+4\eta} + \frac{2}{3} \frac{1}{(1+4\eta)^2} + \frac{2}{5} \frac{1}{(1+4\eta)^3} + \dots, \quad (\eta \gg 1) \\ &= \frac{1}{2\eta} \left(1 - \frac{1}{6\eta} - \frac{11}{120\eta^2} \right) + 0 \left(\frac{1}{\eta^4} \right) \end{aligned} \quad (2.19)$$

from (2.14) and (2.15) we find

$$I_L^{(1)}(\eta \gg 1, \mu \ll 1) = \frac{1}{6\eta} + 0 \left(\frac{1}{\eta^2} \right), \quad (2.20)$$

and

$$I_T^{(1)}(\eta \gg 1, \mu \ll 1) = \frac{1}{3\eta} + 0 \left(\frac{1}{\eta^2} \right), \quad (2.21)$$

as well as

$$I_L^{(1)}(\eta \gg 1, \mu \ll 1) + I_T^{(1)}(\eta \gg 1, \mu \ll 1) = \frac{1}{2\eta} + 0 \left(\frac{1}{\eta^2} \right). \quad (2.22)$$

In this limit of $\eta \gg 1$, the ratio of the longitudinal to the transverse photoabsorption cross section becomes 1/2, [7], [9],

$$R = \frac{\sigma_{\gamma_{Lp}^*}(\eta(W^2, Q^2))}{\sigma_{\gamma_{Tp}^*}(\eta(W^2, Q^2))} = \frac{1}{2}. \quad (2.23)$$

The result (2.23) is a direct consequence of the explicit form of the photon wave function in (2.1). A dependence of the dipole cross section on the product $r_\perp \sqrt{z(1-z)}$ implies [7], [9] helicity independence, the equality of the dipole cross sections (in the limit of $r_\perp^2 \rightarrow 0$) for transversely polarized $q\bar{q}$ states (originating from γ_T^*) and longitudinally polarized ones (originating from γ_L^*). The enhanced transverse size of transverse relative to longitudinal $q\bar{q}$ states calls for a refinement of the simplifying

assumption of helicity independence contained in the ansatz (2.3) and (2.4). The ratio R in (2.23) then becomes [15], [9]

$$R = \frac{1}{2\rho}, \quad (2.24)$$

with $\rho = \text{const} > 1$. Compare Section 2.2 and Appendix A.

ii) The limit of $\eta = c\mu$ with $c = \text{const} \geq 1$, and

- a) $\mu \ll 1$ fixed, $c \rightarrow 1$, the limit of $Q^2 = 0$ photoproduction at fixed energy W ,
- b) $\mu \rightarrow 0$, $\eta = c\mu \rightarrow 0$, $c > 1$ fixed, the limit of $W^2 \rightarrow \infty$ with $Q^2 = (c-1)m_0^2 > 0$ fixed.

Evaluating $I_0(\eta)$ in (2.13) in the limit of $\eta = c\mu \ll 1$, we find the leading term of

$$I_0(\eta) \cong \left(\ln \frac{1}{\eta} \right) \left(1 - 2\eta \left(1 - \frac{1}{\ln \frac{1}{\eta}} \right) \right) \cong \ln \frac{1}{c\mu}, \quad (\eta = c\mu \ll 1). \quad (2.25)$$

Substitution into (2.14) and (2.15) yields

$$\begin{aligned} I_L^{(1)}(\eta = c\mu, c\mu \ll 1) &= \frac{c-1}{c} - 2\mu(c-1) \ln \frac{1}{c\mu} \\ &= \begin{cases} 0 & \text{for } c = 1, (Q^2 = 0, \text{ photopr.}), \\ \frac{c-1}{c} & \text{for } c > 1 \text{ fixed, } \eta = c\mu \rightarrow 0 \\ & (W^2 \rightarrow \infty, Q^2 > 0 \text{ fixed}), \end{cases} \end{aligned} \quad (2.26)$$

and

$$I_T^{(1)}(\eta = c\mu, c\mu \ll 1) = \begin{cases} \ln \frac{1}{\mu} & \text{for } c = 1, (Q^2 = 0, \text{ photopr.}), \\ \ln \frac{1}{c\mu} - \frac{c-1}{c} & \text{for } c > 1 \text{ fixed, } \eta = c\mu \rightarrow 0 \\ & (W^2 \rightarrow \infty, Q^2 > 0 \text{ fixed}). \end{cases} \quad (2.27)$$

The $Q^2 = 0$, photoproduction, results in (2.26) and (2.27), based on the very-high-energy ($\mu(W^2) \ll 1$) representation (2.17), agree with the result (2.10) obtained from (2.9) with $0 < \mu(W^2) < 1$.

In the limit of $W^2 \rightarrow \infty$, but $Q^2 > 0$ fixed i.e. for $c > 1$ fixed and $\eta = c\mu \rightarrow 0$, upon combining (2.26) and (2.27), we find [7, 8, 9] ⁵

$$\lim_{\substack{W^2 \rightarrow \infty \\ Q^2 > 0 \text{ fixed}}} \frac{\sigma_{\gamma^* p}(W^2, Q^2)}{\sigma_{\gamma p}(W^2)} = \lim_{\substack{W^2 \rightarrow \infty \\ Q^2 > 0 \text{ fixed}}} \frac{\sigma_{\gamma_T^* p}(W^2, Q^2)}{\sigma_{\gamma p}(W^2)} = \lim_{\mu \rightarrow 0} \frac{\ln \frac{1}{c\mu}}{\ln \frac{1}{\mu}} = 1. \quad (2.28)$$

At any $Q^2 > 0$, if the energy W is sufficiently large (“saturation limit”), the ratio of the photoabsorption cross section at finite Q^2 over the $Q^2 = 0$ photoabsorption cross section, $\sigma_{\gamma p}(W^2)$, becomes equal to unity. Only the transverse part of the photoabsorption cross section contributes to the ratio (2.28) in this limit of $W^2 \rightarrow \infty$ at $Q^2 > 0$ fixed.

2.2 Refinements

The formulation of the CDP for the photoabsorption cross section in (2.1) to (2.4) implicitly contains contributions from $q\bar{q}$ fluctuations of the (virtual) photon of unlimited mass, $M_{q\bar{q}} \rightarrow \infty$. The life time τ of a $q\bar{q}$ fluctuation, in the rest frame of the target proton of mass M_p [16], [17], [13]

$$\tau \cong \frac{1}{\Delta E} = \frac{1}{x + \frac{M_{q\bar{q}}^2}{W^2}} \frac{1}{M_p}, \quad (2.29)$$

with increasing mass $M_{q\bar{q}}$ decreases strongly, however, at any fixed energy W and any fixed value of $x \cong Q^2/W^2 \lesssim 0.1$. To assure the sufficiently long lifetime of $\tau \gg 1/M_p$ necessary for the validity of the CDP of diffractive $(q\bar{q})p$ forward scattering, the masses of the contributing $q\bar{q}$ fluctuations must be restricted by a W -dependent upper limit, $M_{q\bar{q}}^2 \leq m_1^2(W^2)$.

In ref. [9] we gave a formulation of the photoabsorption cross section in the CDP that incorporates the required upper bound⁶ on $M_{q\bar{q}}^2$,

$$M_{q\bar{q}}^2 \leq m_1^2(W^2) = \xi \Lambda_{sat}^2(W^2). \quad (2.30)$$

Adjustment to the experimental data on DIS showed consistency with the upper limit (2.30) for a constant value of ξ of magnitude of approximately

$$\xi = \text{const} \cong 130. \quad (2.31)$$

⁵Equivalently, one finds (2.28) from (2.9) by inserting $\mu = c\mu$ into (2.9), and evaluating the limit of $\mu \rightarrow 0$ with $c > 1$ fixed.

⁶An upper bound, $M_{q\bar{q}}^2 \leq m_1^2$, was also previously introduced in ref. [18].

The modifications of the longitudinal and the transverse photoabsorption cross sections (2.7) and (2.17) implied by the constraint (2.30) can be cast into simple factors that depend on the ratio

$$u = u(\eta(W^2, Q^2)) = \frac{\xi}{\eta(W^2, Q^2)}. \quad (2.32)$$

The factors, $G_L(u)$ and $G_T(u)$, will be specified below.

The refined formulation of the CDP in ref. [9] also includes the transverse-size enhancement [15] of transversely relative to longitudinally polarized $q\bar{q}$ fluctuations by the factor ρ that was mentioned in (2.24). The factor ρ enters the transverse photoabsorption cross section in (2.17) via the replacement

$$I_T^{(1)}(\eta, \mu) \rightarrow I_T^{(1)}\left(\frac{\eta}{\rho}, \frac{\mu}{\rho}\right), \quad (2.33)$$

compare (A.45) in Appendix A.

Taking into account the constraint (2.30), as well as the transverse-size enhancement factor ρ according to (2.33), the cross sections in (2.7), expressed in terms of the functions $I_L^{(1)}(\eta, \mu)$ and $I_T^{(1)}(\eta, \mu)$ in (2.9) or (2.14) become⁷

$$\begin{aligned} \sigma_{\gamma_L^* p}(W^2, Q^2) &= \frac{\alpha R_{e^+e^-}}{3\pi} \sigma^{(\infty)}(W^2) I_L^{(1)}(\eta, \mu) G_L(u), \\ \sigma_{\gamma_T^* p}(W^2, Q^2) &= \frac{\alpha R_{e^+e^-}}{3\pi} \sigma^{(\infty)}(W^2) I_T^{(1)}\left(\frac{\eta}{\rho}, \frac{\mu}{\rho}\right) G_T(u). \end{aligned} \quad (2.34)$$

For details we refer to Appendix A, specifically see (A.38) and (A.45). The functions $G_L(u)$ and $G_T(u)$ are given by [9]

$$\begin{aligned} G_L(u) &= \frac{2u^3 + 6u^2}{2(1+u)^3} \simeq \begin{cases} 3u^2 & , \quad (u \ll 1), \\ 1 - \frac{3}{u^2} & , \quad (u \gg 1), \end{cases} \\ G_T(u) &= \frac{2u^3 + 3u^2 + 3u}{2(1+u)^3} \simeq \begin{cases} \frac{3}{2}u & , \quad (u \ll 1), \\ 1 - \frac{3}{2u} & , \quad (u \gg 1), \end{cases} \end{aligned} \quad (2.35)$$

where, according to (2.32), the limits of $u(\eta(W^2, Q^2)) \ll 1$ and $u(\eta(W^2, Q^2)) \gg 1$ correspond to the large- η limit of $\eta(W^2, Q^2) \gg \xi$ and the small- η limit of $\eta(W^2, Q^2) \ll \xi$, respectively. According to (2.35), in the large- η limit, $\eta(W^2, Q^2) \gg \xi$, the longitudinal

⁷The compact form of the photoabsorption cross sections in (2.34) is a novel result of the present investigation. Compare Appendix A for its derivation and for the connection with our previous results in ref. [9]

part of the photoabsorption cross section in (2.34) becomes more strongly suppressed than the transverse part.

The total photoabsorption cross section, according to (2.34) is given by

$$\begin{aligned}\sigma_{\gamma^*p}(W^2, Q^2) &= \sigma_{\gamma_L^*p}(W^2, Q^2) + \sigma_{\gamma_T^*p}(W^2, Q^2) = \\ &= \frac{\alpha R_{e^+e^-}}{3\pi} \sigma^{(\infty)}(W^2) \left(I_T^{(1)} \left(\frac{\eta}{\rho}, \frac{\mu}{\rho} \right) G_T(u) + I_L^{(1)}(\eta, \mu) G_L(u) \right).\end{aligned}\tag{2.36}$$

In the photoproduction limit of (2.10), the longitudinal contribution to (2.36) goes to zero, the transverse contribution becomes proportional to $\ln(\rho/\mu(W^2)) = \ln(\rho\Lambda_{sat}^2(W^2)/m_0^2)$, and moreover $G_T(u) \simeq 1$ from (2.35). Requiring consistency of (2.36) in the limit of $Q^2 \rightarrow 0$ with the empirically known photoproduction cross section, allows one to determine the hadronic dipole cross section $\sigma^{(\infty)}(W^2)$. From the $Q^2 \rightarrow 0$ limit of (2.36) we obtain

$$\sigma^{(\infty)}(W^2) = \frac{3\pi}{\alpha R_{e^+e^-}} \frac{1}{\lim_{\eta \rightarrow \mu(W^2)} I_T^{(1)} \left(\frac{\eta}{\rho}, \frac{\mu(W^2)}{\rho} \right)} \sigma_{\gamma p}(W^2).\tag{2.37}$$

For the evaluation of $\sigma^{(\infty)}(W^2)$ the Regge fit to the experimental data for photoproduction, $\sigma_{\gamma p}(W^2)$, [7], [19], or the double-logarithmic fit from the Particle Data Group [20],

$$\begin{aligned}\sigma_{\gamma p}^{(a)}(W^2) &= 0.0635(W^2)^{0.097} + 0.145(W^2)^{-0.5}, \\ \sigma_{\gamma p}^{(b)}(W^2) &= 0.0677(W^2)^{0.0808} + 0.129(W^2)^{-0.4525}, \\ \sigma_{\gamma p}^{(c)}(W^2) &= 0.003056 \left(33.71 + \frac{\pi}{M^2} \ln^2 \frac{W^2}{(M_p + M)^2} \right) + 0.0128 \left(\frac{(M_p + M)^2}{W^2} \right)^{0.462},\end{aligned}\tag{2.38}$$

(where M_p stands for the proton mass and $M \equiv 2.15 \text{ GeV}$) are to be inserted into (2.37).

The $(\ln W^2)^2$ dependence of $\sigma_{\gamma p}^{(c)}(W^2)$ in (2.38) together with (2.27) implies a growth of $\sigma^{(\infty)}(W^2)$ in (2.37) as $\sigma^{(\infty)}(W^2) \sim \ln W^2$. The photoabsorption cross section (2.36) for fixed $Q^2 \geq 0$, taking into account (2.26) as well as $I_T^{(1)} \sim \ln W^2$ from (2.27), then grows as $(\ln W^2)^2$. The photoabsorption cross section at any fixed $Q^2 \geq 0$ for $W^2 \rightarrow \infty$ behaves hadronlike, compare also (2.28) [7], [8].

The growth of the photoabsorption cross section with increasing energy as $(\ln W^2)^2$, for any fixed $Q^2 \geq 0$, coincides with the hadronic $(\ln W^2)^2$ behavior conjectured by

Heisenberg [21] for cross sections among strongly interacting particles, and recognized as the maximal possible growth with energy by Froissart [22]. We note that a hadronlike Froissart-like saturation behavior of $\sigma_{\gamma^*p}(W^2, Q^2)$ for W^2 sufficiently large, $Q^2 \geq 0$ fixed, was recently also demonstrated [23] by the success of an explicit ‘‘Froissart-inspired’’ fit to the DIS experimental data for $x \cong \frac{Q^2}{W^2} \leq 0.1$.

We turn to a discussion of the longitudinal-to-transverse ratio $R(W^2, Q^2)$. According to (2.34), it is given by

$$R(W^2, Q^2) = \frac{\sigma_{\gamma_L^*p}(W^2, Q^2)}{\sigma_{\gamma_T^*p}(W^2, Q^2)} = \frac{I_L^{(1)}(\eta, \mu)}{I_T^{(1)}\left(\frac{\eta}{\rho}, \frac{\mu}{\rho}\right)} \frac{G_L(u)}{G_T(u)}. \quad (2.39)$$

In the $Q^2 = 0$ photoproduction limit of $\eta(W^2, Q^2 = 0) = \mu(W^2) \ll 1$ (as a consequence of electromagnetic gauge invariance), the ratio $R(W^2, Q^2)$ becomes zero. For $\eta(W^2, Q^2) \gg 1$, according to (2.20) and (2.21),

$$R(W^2, Q^2) = \frac{1}{2\rho} \frac{G_L(u)}{G_T(u)}, \quad (\eta(W^2, Q^2) \gg 1). \quad (2.40)$$

The (necessary) restriction (2.30) on the mass, $M_{q\bar{q}}$, of $q\bar{q}$ fluctuations modifies (2.24) to become (2.40). In the region of $u(\eta(W^2, Q^2)) = \xi/\eta(W^2, Q^2) \gg 1$, according to (2.35), we have $G_L(u)/G_T(u) \cong 1$ in (2.40). For $u(\eta(W^2, Q^2)) \ll 1$, we have $G_L(u)/G_T(u) \simeq 2u = 2\xi/\eta$ corresponding to a strong decrease of $R(W^2, Q^2)$ for sufficiently large Q^2 at fixed energy W .

A measurement of $R(W^2, Q^2)$ for Q^2 sufficiently large determines the magnitude of ρ . The parameter ρ , according to (A.42) to (A.44), is to be identified with the ratio of the cross sections for transversely polarized, $(q\bar{q})_T^{J=1}$, and longitudinally polarized, $(q\bar{q})_L^{J=1}$, dipole states in the limit of vanishing dipole size, $\vec{r}_\perp'^2 \rightarrow 0$,

$$\rho = \frac{\bar{\sigma}_{(q\bar{q})_T^{J=1}p}(\vec{r}_\perp'^2, W^2)}{\bar{\sigma}_{(q\bar{q})_L^{J=1}p}(\vec{r}_\perp'^2, W^2)} \Big|_{\vec{r}_\perp'^2 \rightarrow 0}. \quad (2.41)$$

The proportionality of the dipole cross sections in (2.41) to the (transverse) size $\vec{r}_\perp'^2$ of the $(q\bar{q})_{L,T}^{J=1}$ dipole states implies that ρ is independent of the energy W of the $(q\bar{q})p$ interaction.

According to (A.39) to (A.44), transverse $q\bar{q}$ states, $(q\bar{q})_T^{J=1}$, (for $\rho > 1$) interact with enhanced transverse size compared with $(q\bar{q})_L^{J=1}$ states,

$$\bar{\sigma}_{(q\bar{q})_T^{J=1}p}(\vec{r}_\perp'^2, W^2) = \bar{\sigma}_{(q\bar{q})_L^{J=1}p}(\rho \vec{r}_\perp'^2, W^2), \quad (\vec{r}_\perp'^2 \rightarrow 0). \quad (2.42)$$

The parameter ρ directly measures the effect of the enhanced transverse size of transversely relative to longitudinally polarized $q\bar{q}$ states. The prediction [15], [9] of

$$\rho = \frac{4}{3} \quad (2.43)$$

is based on the assumption that the effect of the enhanced transverse size can be fully taken care of by employing the average transverse sizes of $(q\bar{q})_T^{J=1}$ and $(q\bar{q})_L^{J=1}$ states, when predicting the relative magnitude of their cross sections. A deviation from the prediction (2.43) is to be interpreted as a dependence of the interaction of $q\bar{q}$ states with the proton that is not fully taken care of by employing the average sizes of the $q\bar{q}$ states. A deviation from (2.43) thus indicates an additional dependence on the $z(1-z)$ internal configuration of $(q\bar{q})^{J=1}$ states not incorporated in the averaging procedure leading to $\rho = 4/3$.

According to the preceding discussion it is clear that the general formulation of the CDP in (2.1) and (2.2) implies $\rho = \text{const}$ due to invariance under Lorentz boosts. Deviations from the prediction (2.43) for the numerical value of $\rho = 4/3$ from (2.43) cannot be strictly excluded. In ref. [9], we introduced a more general ansatz for the dipole cross section that leads to a parameter-dependent expression for $\rho = \rho(\epsilon \equiv 1/6a)$. According to (A.46), we have [9]

$$\rho(\epsilon \equiv 1/6a) = \begin{cases} 1 & \text{for } a = 2.54, \\ \frac{4}{3} & \text{for } a = 5.53, \\ 2 & \text{for } a = 23.2. \end{cases} \quad (2.44)$$

The general ansatz from ref. [9] thus contains helicity independence, $\rho = 1$, as well as the required enhanced-transverse-size effect of $\rho > 1$.

3 Theory versus experiment

In the present section we present the theoretical results from Section 2 in a form that is convenient to be employed in a fit to the experimental data. In particular, we present the theoretical results in terms of the so-called reduced cross section employed in the recent combined analysis of the H1- and ZEUS collaborations [24]. We also elaborate on how the photoproduction limit should be tested by the experimental data, and we present a comparison of the longitudinal-to-transverse ratio $R(W^2, Q^2)$ with experimental data.

According to (2.36) and (2.37), we have

$$\sigma_{\gamma^*p}(W^2, Q^2) = \frac{\sigma_{\gamma p}(W^2)}{\lim_{\eta \rightarrow \mu(W^2)} I_T^{(1)}\left(\frac{\eta}{\rho}, \frac{\mu(W^2)}{\rho}\right)} \left(I_T^{(1)}\left(\frac{\eta}{\rho}, \frac{\mu}{\rho}\right) G_T(u) + I_L^{(1)}(\eta, \mu) G_L(u) \right). \quad (3.1)$$

$I_{L,T}^{(1)}(\eta, \mu)$ and $G_{L,T}(u)$ are given in (2.9) or (2.14) and (2.35), respectively. According to (2.9)

$$\lim_{\eta \rightarrow \mu(W^2)} I_T^{(1)}\left(\frac{\eta}{\rho}, \frac{\mu(W^2)}{\rho}\right) = \ln \frac{\rho}{\mu(W^2)}, \quad (3.2)$$

while according to (2.14)

$$\begin{aligned} \lim_{\eta \rightarrow \mu(W^2)} I_T^{(1)}\left(\frac{\eta}{\rho}, \frac{\mu(W^2)}{\rho}\right) &= I_0\left(\frac{\mu(W^2)}{\rho}\right) \\ &\cong \ln \frac{\rho}{\mu(W^2)} \left(1 - 2\frac{\mu}{\rho} \left(1 - \frac{1}{\ln \frac{\rho}{\mu}} \right) \right) < \ln \frac{\rho}{\mu(W^2)}. \end{aligned} \quad (3.3)$$

For the photoproduction cross section, $\sigma_{\gamma p}(W^2)$, in (3.1) the empirical fit in (2.38) is to be inserted. Independently of whether (2.9) or (2.14) is employed in (3.1), we have convergence to the photoproduction $\lim_{Q^2 \rightarrow 0} \sigma_{\gamma^*p}(W^2, Q^2) = \sigma_{\gamma p}(W^2)$ in (3.1). The somewhat smaller value of $I_T^{(1)}(\eta, \mu)$ in the limit of $\eta \rightarrow \mu$ in (3.3) compared with (3.2) at $\eta \gg 1$ leads to a slightly larger cross section (3.1) for the case of (2.14) that may be absorbed into a somewhat smaller value of ξ in $m_1^2(W^2) = \xi \Lambda_{sat}^2(W^2)$.

The longitudinal-to-transverse ratio $R(W^2, Q^2)$, according to (2.39) as well as (3.1), becomes

$$R(W^2, Q^2) = \frac{\sigma_{\gamma_L^*p}(W^2, Q^2)}{\sigma_{\gamma_T^*p}(W^2, Q^2)} = \frac{I_L^{(1)}(\eta, \mu) G_L(u)}{I_T^{(1)}\left(\frac{\eta}{\rho}, \frac{\mu}{\rho}\right) G_T(u)}. \quad (3.4)$$

From (2.35), one finds that the factor $G_L(u)/G_T(u)$ in (3.4) is given by

$$\frac{G_L(u)}{G_T(u)} \cong \begin{cases} 1 + \frac{3}{2u} = 1 + \frac{3}{2} \frac{\eta(W^2, Q^2)}{\xi} & , \text{ for } \eta \ll \xi, \\ 2u = 2 \frac{\xi}{\eta(W^2, Q^2)} & , \text{ for } \eta \gg \xi. \end{cases} \quad (3.5)$$

For $Q^2 = 0$ photoproduction, $\eta(W^2, Q^2) = \mu(W^2)$, according to (2.26) and (2.27), the ratio $I_L^{(1)}(\eta, \mu)/I_T^{(1)}(\eta, \mu)$ in (3.4) goes to zero,

$$R(W^2, Q^2 = 0) = 0. \quad (3.6)$$

For $\eta(W^2, Q^2) \gg 1$, from (2.20) and (2.21), we find

$$R(W^2, Q^2) \cong \frac{1}{2\rho} \frac{G_L(u)}{G_T(u)}, \quad (\eta \gg 1), \quad (3.7)$$

and upon substituting (3.5),

$$R(W^2, Q^2) \cong \frac{1}{2\rho} \begin{cases} (1 + \frac{3}{2}\frac{\eta}{\xi}) & , \quad \text{for } 1 \ll \eta \ll \xi, \\ \frac{\xi}{\eta} & , \quad \text{for } \eta \gg \xi. \end{cases} \quad (3.8)$$

The ratio $R(W^2, Q^2)$, for e.g. fixed energy W , with increasing $\eta \cong Q^2/\Lambda_{sat}^2(W^2)$ increases proportional to Q^2 , and upon reaching a maximum decreases inversely proportional to Q^2 as $1/\eta \cong \Lambda_{sat}^2(W^2)/Q^2$. In the approximation of ignoring the finiteness of $m_1^2(W^2)$, for $\xi \rightarrow \infty$, we have $R \cong 1/2\rho$ for sufficiently large $\eta(W^2, Q^2) \gg \mu(W^2)$.

The total photoabsorption cross section in (3.1) and the ratio $R(W^2, Q^2)$ in (3.4) depend on the numerical values of the saturation scale $\Lambda_{sat}^2(W^2)$, and the lower and upper bounds, m_0^2 and $m_1^2(W^2) = \xi\Lambda_{sat}^2(W^2)$, on the masses of the $q\bar{q}$ fluctuations. The saturation scale is determined by its normalization C_1 and the exponent C_2 ,

$$\Lambda_{sat}^2(W^2) = C_1 \left(\frac{W^2}{1GeV^2} \right)^{C_2}. \quad (3.9)$$

Compare also the previously employed [7] form

$$\Lambda_{sat}^2(W^2) = B \left(1 + \left(\frac{W^2}{W_0^2} \right) \right)^{C_2} \cong C_1 \left(\frac{W^2}{1GeV^2} \right)^{C_2}. \quad (3.10)$$

The successful representation of the experimental data in [9] was based on

$$\begin{aligned} B &= 2.04GeV^2, \\ W_0^2 &= 1081GeV^2, \\ C_2 &= 0.27, \\ m_0^2 &= 0.15GeV^2, \\ \xi &= 130. \end{aligned} \quad (3.11)$$

The parameter ρ , from an estimate [15, 9] based on the uncertainty relation as applied to the different $z(1-z)$ configurations of $q\bar{q}$ states from $\gamma_L^* \rightarrow q\bar{q}$ and $\gamma_T^* \rightarrow q\bar{q}$, was determined to be $\rho = 4/3$.

In fig. 3.1, we compare the results from the simple closed expression for the photoabsorption cross section in (3.1) with the previous more involved form evaluated in [9], and we find good agreement. The evaluation of the cross section (3.1) was carried out with

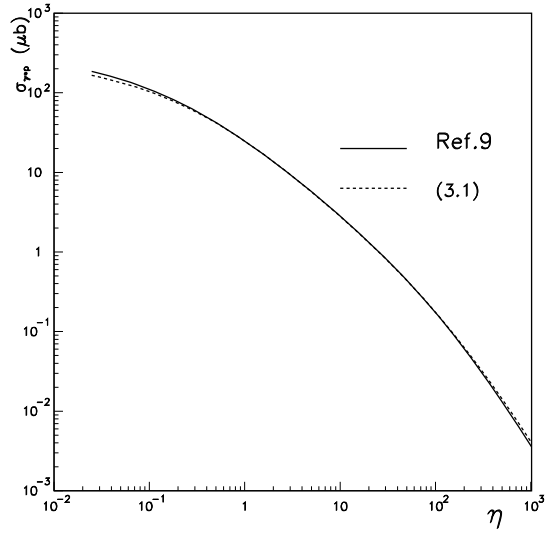


Figure 3.1: Comparison of the photoabsorption cross section based on the simple closed analytic expression (3.1) with the result from ref. [9]

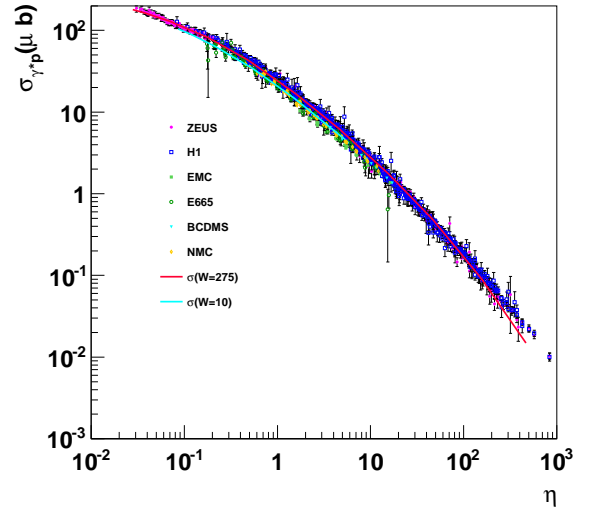


Figure 3.2: Comparison of the photoabsorption cross section with experiment, as shown in ref. [9]

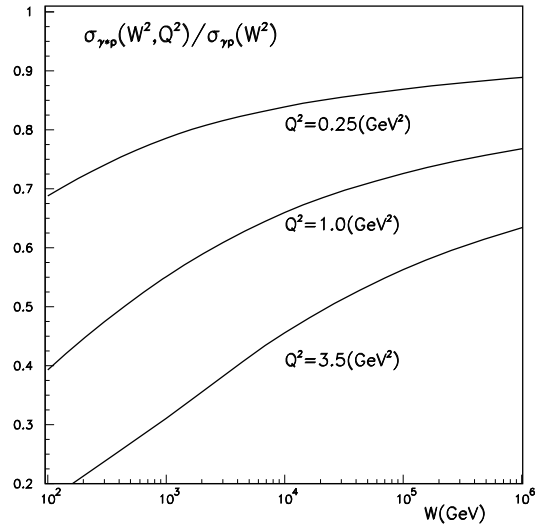


Figure 3.3: The W dependence of the ratio (2.28) of $\sigma_{\mu p}(W^2, Q^2)/\sigma_{\gamma p}(W^2)$ for several values of Q^2 showing the slow convergence to the hadronlike dependence of $\sigma_{\gamma p}(W^2) \sim (\ln W^2)^2$ for any fixed value of $Q^2 > 0$.

the numerical values of the parameters given in (3.11). For easy reference, in fig. 3.2, we reproduce the comparison with experiment shown in fig. 9 of ref. [9].

The results shown in fig. 3.3 are relevant for the asymptotic behavior [7], [8], [9] of the photoabsorption cross section, $\sigma_{\gamma^*p}(W^2, Q^2)/\sigma_{\gamma p}(W^2) \rightarrow 1$ for $W^2 \rightarrow \infty$, as given by (2.28). Dividing (3.1) by the $Q^2 = 0$ photoproduction cross section, we show the ratio of $\sigma_{\gamma^*p}(W^2, Q^2)/\sigma_{\gamma p}(W^2)$ as a function of W for various values of Q^2 . The figure illustrates the very slow approach to the saturation limit of photoproduction. The slow approach to this unique limit of the theoretically well-founded CDP differs strongly from the results of an *ad hoc* fit⁸ presented more recently in ref. [25]. The high-energy extrapolation of this *ad hoc* fit at fixed Q^2 leads to a break down of the fit (“crossing”) for values of x around $x \simeq 10^{-8}$ corresponding to $W \simeq 10^4 \text{ GeV}$ to $W \simeq 10^5 \text{ GeV}$.

The H1 and ZEUS Collaborations have recently presented [24] a combined analysis of their measurements on electron (positron)-proton scattering carried out at the ep collider HERA from 1992 to 2007. The results of the experiment are given in terms of the so-called reduced cross sections [24]

$$\sigma_{r,NC}^{\pm} = \frac{d^2\sigma_{NC}^{e^{\pm}p}}{dx_{Bj}dQ^2} \frac{Q^4 x_{Bj}}{2\pi\alpha^2 Y_+}, \quad (3.12)$$

where NC refers to the neutral-current electron (positron) scattering process. In the case of $Q^2 \ll M_Z^2$ we are concerned with in the present note, the reduced cross section is related to the proton electromagnetic structure functions $F_2(x, Q^2)$ and $F_L(x, Q^2)$ via

$$\begin{aligned} \sigma_{r,NC}^{\pm} &\equiv \sigma_r(Q^2, x_{bj}, s) \\ &= F_2(x, Q^2) - \frac{y^2}{1 + (1 - y)^2} F_L(x, Q^2), \end{aligned} \quad (3.13)$$

where $x \equiv x_{bj}$, $Q^2 = -q^2 > 0$ with q^2 being the four-momentum transfer from the electron (positron) to the proton, and y denotes the ratio of the hadronic center-of-mass energy squared, W^2 , to the total $e^{\pm}p$ energy squared, s . In detail,

$$x_{bj} \equiv x = \frac{Q^2}{W^2 + Q^2 - M_p^2} \cong \frac{Q^2}{W^2}, \quad (3.14)$$

and

$$y = \frac{Q^2}{sx} \cong \frac{W^2}{s}, \quad Y_+ = 1 + (1 - y)^2. \quad (3.15)$$

⁸Neither the underlying approximation of $\tau \approx 1/x$, ignoring $M_{q\bar{q}}^2$ in (2.29) employed in [25], nor the assumed power-law dependence of $\sigma_{\gamma^*p} \sim (1/x)^{\lambda(Q^2)}$ is based on theoretical principles.

The precision experimental data [24] call for a detailed examination of the low x region, $x \lesssim 0.1$, and in particular for a close examination of the important $Q^2 \rightarrow 0$ photoproduction limit that is excluded in the analysis of reference [24].

The pair of variables relevant at low values of $x \lesssim 0.1$ is the pair (Q^2, W^2) , since the transition to $Q^2 = 0$ photoproduction requires $Q^2 \rightarrow 0$ at fixed W^2 .⁹ It is also appropriate to replace the structure functions $F_2(x, Q^2)$ and $F_L(x, Q^2)$ by the photoabsorption cross sections for transversely and longitudinally polarized (virtual) photons [26] $\sigma_{\gamma_T^* p}(W^2, Q^2)$ and $\sigma_{\gamma_L^* p}(W^2, Q^2)$, via

$$F_2 = \frac{Q^2}{4\pi^2\alpha} \left(\sigma_{\gamma_T^* p}(W^2, Q^2) + \sigma_{\gamma_L^* p}(W^2, Q^2) \right), \quad (3.16)$$

and

$$F_L = \frac{Q^2}{4\pi^2\alpha} \sigma_{\gamma_L^* p}(W^2, Q^2), \quad (3.17)$$

where, for the presently relevant case of $W^2 \gg Q^2$ as well as $W^2 \gg M_p^2$ (with M_p denoting the proton mass), in (3.16) and (3.17) the approximation

$$\frac{Q^4(1-x)}{4\pi^2\alpha(Q^2 + (2M_p x)^2)} \cong \frac{Q^2}{4\pi^2\alpha} \quad (3.18)$$

was inserted. Replacing the structure functions in (3.13) by the photoabsorption cross sections according to (3.16) and (3.17), with

$$\sigma_{\gamma^* p}(W^2, Q^2) \equiv \sigma_{\gamma_T^* p}(W^2, Q^2) + \sigma_{\gamma_L^* p}(W^2, Q^2) \quad (3.19)$$

and

$$R(W^2, Q^2) \equiv \frac{\sigma_{\gamma_L^* p}(W^2, Q^2)}{\sigma_{\gamma_T^* p}(W^2, Q^2)}, \quad (3.20)$$

we obtain

$$\begin{aligned} \frac{4\pi^2\alpha}{Q^2} \sigma_r(W^2, Q^2, s) &= \sigma_{\gamma_T^* p}(W^2, Q^2) \left(1 + \left(1 - \frac{y^2}{1 + (1-y)^2} \right) R(W^2, Q^2) \right) \\ &= \sigma_{\gamma^* p}(W^2, Q^2) \left(1 + \frac{y^2}{1 + (1-y)^2} \frac{R(W^2, Q^2)}{1 + R(W^2, Q^2)} \right). \end{aligned} \quad (3.21)$$

Since y^2 and $R(W^2, Q^2)$ are small compared with unity, the main contributions from the right-hand side in (3.21) are due to the first terms in the brackets. With $R(W^2, Q^2) \rightarrow 0$

⁹The limit $Q^2 \rightarrow 0$ at fixed W^2 in the pair of variables (Q^2, x) corresponds to the (less convenient) transition of $Q^2 \rightarrow 0$ at fixed values of Q^2/x , where $Q^2/x = W^2 - M_p^2 = \text{const}$ is to be required.

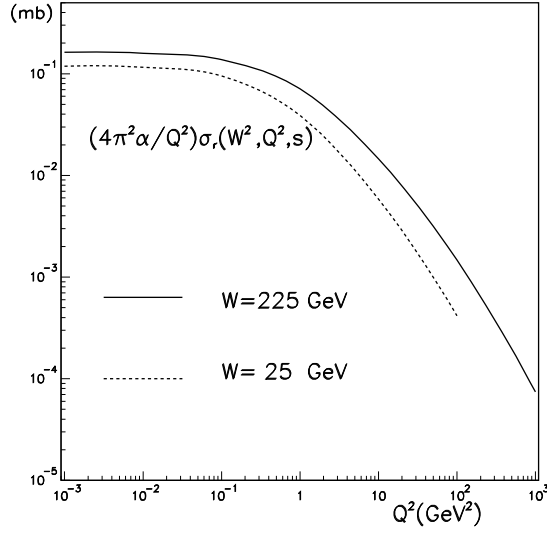


Figure 3.4: The theoretical results for the reduced cross section multiplied by $4\pi^2\alpha/Q^2$, compare (3.19) to (3.21), as a function of Q^2 for fixed W at $\sqrt{s} = 318$ GeV.

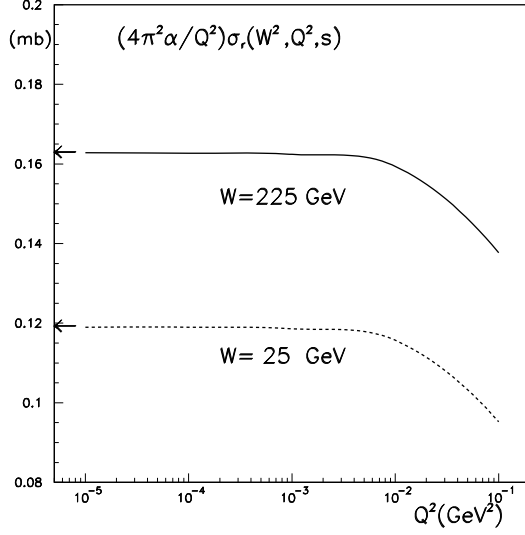


Figure 3.5: Same as fig. 3.4, but for $Q^2 < 0.1$ GeV²

as a consequence of electromagnetic gauge invariance, photoproduction, $\sigma_{\gamma p}(W^2)$ from (3.21), is obtained via

$$\lim_{\substack{Q^2 \rightarrow 0 \\ W^2 \text{ fixed}}} \frac{4\pi^2\alpha}{Q^2} \sigma_r(W^2, Q^2, s) = \sigma_{\gamma p}(W^2). \quad (3.22)$$

The experimental results from reference [24], given for ep energies of $\sqrt{s} = 318$ GeV, 300 GeV and 251 GeV in bins of (Q^2, x) , have to be converted into bins of (Q^2, W^2) . The corresponding very elaborate analysis is better carried out by the experimentalists responsible for these data [24].

In figs. 3.4 and 3.5, we present the theoretical results for the reduced cross section at $\sqrt{s} = 318$ GeV multiplied by $4\pi^2\alpha/Q^2$, compare (3.21). The photoabsorption cross section and the ratio $R(W^2, Q^2)$ entering (3.21) are obtained by evaluating (3.1) and (3.4) with the parameters given in (3.11) and used for figs. 3.1 to 3.3. More specifically, in fig. 3.4 we show the theoretical results for the cross section (3.21) for fixed W^2 as a function of Q^2 , Q^2 being restricted by $x \cong Q^2/W^2 < 0.1$. In fig. 3.5, we concentrate on the region of very small Q^2 , in order to examine the $Q^2 = 0$ limit of photoproduction in more detail.

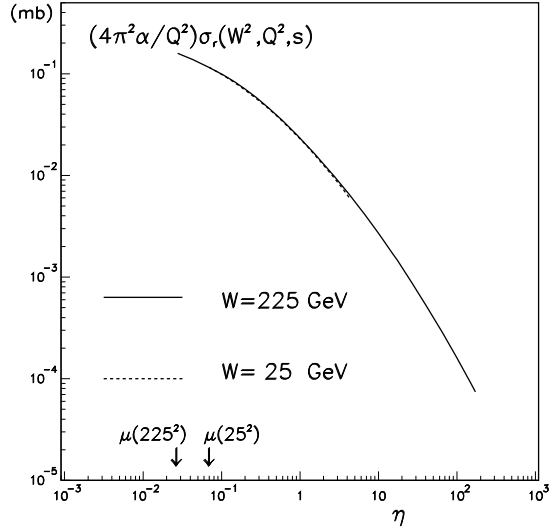


Figure 3.6: Scaling of $(4\pi^2\alpha/Q^2)\sigma^r(W^2, Q^2)$ in the low-x scaling variable $\eta(W^2, Q^2)$, compare (3.23) as well as (3.26) and (3.21). As in figs. 3.4 and 3.5, $\sqrt{s} = 318 \text{ GeV}$.

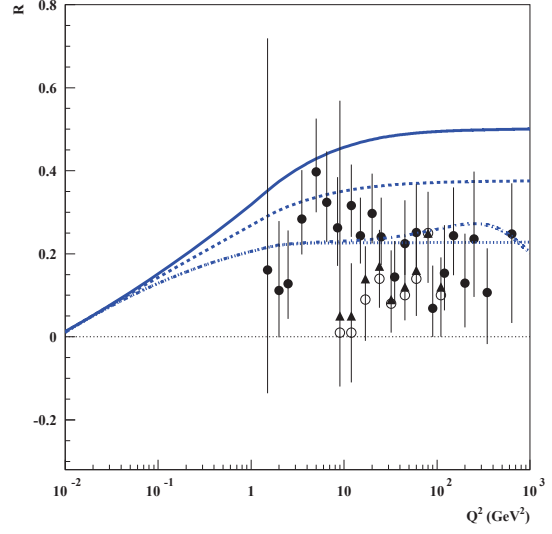


Figure 3.7: The experimental values of $R(W^2, Q^2)$ at $W \simeq 200 \text{ GeV}$ compared with the prediction from the CDP. The curves correspond to $\rho = 1$, $\rho = 4/3$ and $\rho = 2$, respectively.

In fig. 3.6, we show the theoretical results for the reduced cross section multiplied by $4\pi^2\alpha/Q^2$, compare (3.21), as a function of the low-x scaling variable, (2.5) and (3.9),

$$\eta(W^2, Q^2) \equiv \frac{Q^2 + m_0^2}{\Lambda_{sat}^2(W^2)}, \quad (3.23)$$

where

$$\Lambda_{sat}^2(W^2) = C_1 \left(\frac{W^2}{1 \text{ GeV}^2} \right)^{C_2} \quad (3.24)$$

with

$$\begin{aligned} m_0^2 &= 0.15 \text{ GeV} \\ C_1 &= 0.31 \\ C_2 &= 0.27 \end{aligned} \quad (3.25)$$

Since the second term in the bracket on the right-hand side in (3.21) is small, the prediction [7] from the color-dipole picture (CDP) of low-x scaling,

$$\sigma_{\gamma^*p}(W^2, Q^2) = \sigma_{\gamma^*p}(\eta(W^2, Q^2)), \quad (3.26)$$

is approximately valid for $\sigma_r(Q^2, W^2, s)$.

We turn to the comparison of our prediction for $R(W^2, Q^2)$, given in (3.6) to (3.8), with the H1 and ZEUS experimental results [27]. In a first step, we ignore the upper limit on $m_1^2(W^2)$ by adopting $\xi \rightarrow \infty$. According to (3.6) and (3.8),

$$R(W^2, Q^2) \rightarrow \begin{cases} 0 & , \text{ for } Q^2 \rightarrow 0, \\ \frac{1}{2\rho} & , \text{ for } \eta \simeq \frac{Q^2}{\Lambda_{sat}^2(W^2)} \gg 1. \end{cases} \quad (3.27)$$

For the experimental data from H1 and ZEUS belonging to fixed W of $W \cong 200$ GeV, the condition of $\eta(W^2, Q^2) \gg 1$ in (3.27) is fulfilled for $Q^2 \gg 10$. We accordingly predict

$$R(W^2 \simeq (200 \text{ GeV})^2, Q^2) \rightarrow \begin{cases} 0 & , \text{ for } Q^2 \rightarrow 0, \\ \frac{1}{2\rho} & , \text{ for } Q^2 \gg 10 \text{ GeV}^2 \end{cases} \quad (3.28)$$

i.e. an approach to a constant value of $R \cong 1/2\rho$ for sufficiently large Q^2 . We recall that the factor $1/2$ in (3.28) originates from the ratio of the total $\gamma^*(q\bar{q})$ transition strengths for longitudinally and transversely polarized photons, while ρ stands for the enhanced cross section for transversely relative to longitudinally polarized $q\bar{q}$ states. From an estimate based on the uncertainty principle, we predicted $\rho = 4/3$ [15, 9].

The experimental results in fig.3.7¹⁰ are consistent¹¹ with the prediction (3.28). Previous experimental data [9] showed consistency for $R(W^2, Q^2)$ based on $\rho = 4/3$. The present more accurate experimental data demonstrate the expected approach to a constant value of ρ , but they require the larger value of $\rho \cong 2$. The transverse-size enlargement is somewhat larger than the prediction of $\rho = 4/3$ from the uncertainty principle. This indicates that the interaction mechanism of the $q\bar{q}$ dipole with the gluon field in the nucleon cannot be fully reduced to a different value of the average of the $z(1-z)$ distribution (compare (A.39) and (A.40)), when passing from longitudinally to transversely polarized $q\bar{q}$ states.

4 Conclusion.

The total photoabsorption cross section is determined by the imaginary part of the (virtual) Compton-forward-scattering amplitude. At low values of the Bjorken scaling variable $x \lesssim 0.1$, the imaginary part of the forward-scattering amplitude factorizes into a

¹⁰Figure 3.7 was prepared by B. Surrow.

¹¹In Fig. 3.7, we also show that the result of taking into account $\xi = 130$ is negligible in the presently investigated kinematic saturation.

transition of the photon to quark-antiquark pairs and their subsequent forward scattering in the gluon field of the nucleon. The gauge-invariant coupling of the quark-antiquark color dipole to gluons, at any fixed center-of-mass energy W , implies a hadron-like energy dependence of the cross section at small values of the photon virtuality, and a stronger increase with W at large values of the photon virtuality, where the dipole acts as a color-neutral state. The dependence on the relative magnitude of Q^2 and W^2 implies the observed low- x scaling behavior in terms of the scaling variable $\eta(W^2, Q^2)$. At any fixed Q^2 , at sufficiently high energy W , the transition occurs from color transparency to hadron-like behavior.

It has been the aim of the present paper to reduce the formalism of the CDP to most simple closed analytic expressions for the photoabsorption cross section for transversely and longitudinally polarized photons. The resulting total cross section agrees with experimental data. A detailed global analysis of all experimental data on the basis of our theoretical results is better carried out by the experimental groups responsible for most of the high-energy experimental results.

With respect to the longitudinal-to-transverse ratio, $R(W^2, Q^2)$, our predictions are consistent with the approximate constancy observed at sufficiently large Q^2 . The absolute magnitude of $R(W^2, Q^2) = 1/(2\rho)$, where the factor ρ is due to the enhanced transverse size of transversely relative to longitudinally polarized dipole states, shows that the experimental value of $\rho \cong 2$ is somewhat larger than the estimate from the uncertainty principle of $\rho \cong 4/3$. This implies that the difference in the cross sections of transversely-versus-longitudinally polarized dipole states cannot be fully reduced to the simple picture of average transverse sizes without a more detailed consideration of the effect of the different quark and antiquark transverse momenta in the quark-antiquark dipole states.

Appendix A. Details on the Derivation of the Photoabsorption Cross Section (2.34).

In this Appendix, we provide a brief exposition of the derivation¹² of the photoabsorption cross sections (2.34) and (2.36) which incorporate the upper limit $M_{q\bar{q}}^2 \leq m_1^2(W^2)$, compare

¹²The present derivation expands and improves the treatment in Appendix C of ref. [9].

(2.30), on the mass, $M_{q\bar{q}}$, of $q\bar{q}$ fluctuations of the (virtual) photon.

We also elaborate on the introduction of the transverse-size-enhancement factor ρ in (2.24) and (2.33).

Upon transition to momentum space, and upon introducing the mass variables

$$M^2 = \frac{\vec{k}_\perp^2}{z(1-z)}, \quad M'^2 = \frac{(\vec{k}_\perp + \vec{l}_\perp)^2}{z(1-z)}, \quad (\text{A.1})$$

for $q\bar{q}$ states, as well as

$$\vec{l}_\perp'^2 = \frac{\vec{l}_\perp^2}{z(1-z)}, \quad (\text{A.2})$$

where \vec{k}_\perp and \vec{l}_\perp refer to transverse three momenta of (massless) quarks and gluons, the photoabsorption cross sections in (2.1) with (2.2) become [6, 7, 9]

$$\begin{aligned} \sigma_{\gamma_{Lp}^*}(W^2, Q^2) &= \frac{\alpha R_{e^+e^-}}{3\pi} \int d\vec{l}_\perp'^2 \bar{\sigma}_{(q\bar{q})_L^{J=1p}}(\vec{l}_\perp'^2, W^2) \\ &\times \int dM^2 \int dM'^2 w(M^2, M'^2, \vec{l}_\perp'^2) \\ &\times Q^2 \left(\frac{1}{(Q^2 + M^2)^2} - \frac{1}{(Q^2 + M^2)(Q^2 + M'^2)} \right) \end{aligned} \quad (\text{A.3})$$

and

$$\begin{aligned} \sigma_{\gamma_{Tp}^*}(W^2, Q^2) &= \frac{\alpha R_{e^+e^-}}{3\pi} \int d\vec{l}_\perp'^2 \bar{\sigma}_{(q\bar{q})_T^{J=1p}}(\vec{l}_\perp'^2, W^2) \\ &\times \int dM^2 \int dM'^2 w(M^2, M'^2, \vec{l}_\perp'^2) \\ &\times \left(\frac{M^2}{(Q^2 + M^2)^2} - \frac{M^2 + M'^2 - \vec{l}_\perp'^2}{2(Q^2 + M^2)(Q^2 + M'^2)} \right). \end{aligned} \quad (\text{A.4})$$

In the transition from (2.1) and (2.2) to (A.3) and (A.4), we introduced the cross sections $\bar{\sigma}_{(q\bar{q})_L^{J=1p}}(\vec{l}_\perp'^2, W^2)$ and $\bar{\sigma}_{(q\bar{q})_T^{J=1p}}(\vec{l}_\perp'^2, W^2)$ for the scattering of longitudinally and transversely polarized $J = 1$ $q\bar{q}$ (vector) states on the proton. The quantity $R_{e^+e^-}$ is given by $R_{e^+e^-} = 3\sum_q Q_q^2$, the sum over q running over the squares of the charges of the actively contributing quark flavors ($\sum_q Q_q^2 = 10/9$ for four active flavors). The Jacobian $w(M^2, M'^2, \vec{l}_\perp'^2)$ in (A.3) and (A.4) is given by [6, 7, 9]

$$w(M^2, M'^2, \vec{l}_\perp'^2) = \frac{1}{2MM'\sqrt{1 - \cos^2\phi}} = \frac{1}{2M\sqrt{\vec{l}_\perp'^2}\sqrt{1 - \cos^2\vartheta}}, \quad (\text{A.5})$$

where ϕ denotes the angle between \vec{k}_\perp and $\vec{k}_\perp + \vec{l}_\perp$, and ϑ denotes the angle between \vec{k}_\perp and \vec{l}_\perp . Since

$$\cos^2 \phi = \frac{1}{4M^2 M'^2} (M^2 + M'^2 - \vec{l}_\perp'^2)^2 \quad (\text{A.6})$$

in (A.5) is symmetric under exchange of M^2 and M'^2 , also $w(M^2, M'^2, \vec{l}_\perp'^2)$ in (A.5) is symmetric under this exchange.

Noting that

$$M'^2(M^2, \vec{l}_\perp'^2, \cos \vartheta) = M^2 + \vec{l}_\perp'^2 + 2M\sqrt{\vec{l}_\perp'^2} \cos \vartheta \quad (\text{A.7})$$

and

$$\frac{\partial M'^2(M^2, \vec{l}_\perp'^2, \cos \vartheta)}{\partial \vartheta} = \frac{-1}{w(M^2, M'^2, \vec{l}_\perp'^2)} \quad (\text{A.8})$$

the integrations in (A.3) and (A.4) over dM^2 and dM'^2 may be replaced by integrations over dM^2 and $d\vartheta$,

$$\begin{aligned} \int dM^2 \int dM'^2 w(M^2, M'^2, \vec{l}_\perp'^2) &= \int_{m_0^2}^{m_1^2(W^2)} dM^2 \int_0^\pi d\vartheta - \int_{(\sqrt{\vec{l}_\perp'^2} - m_0)^2}^{(\sqrt{\vec{l}_\perp'^2} + m_0)^2} dM^2 \int_{\vartheta_0(M^2, \vec{l}_\perp'^2)}^\pi d\vartheta \\ &- \int_{(m_1(W^2) - \sqrt{\vec{l}_\perp'^2})^2}^{m_1^2(W^2)} dM^2 \int_0^{\vartheta_1(M^2, \vec{l}_\perp'^2)} d\vartheta. \end{aligned} \quad (\text{A.9})$$

The bounds

$$m_0^2 \leq M^2, M'^2(M^2, \vec{l}_\perp'^2, \cos \vartheta) \leq m_1^2(W^2) \quad (\text{A.10})$$

lead to three terms, as indicated in (A.9). The first term in (A.9) takes care of the bound (A.10) on M^2 , and the second and third terms correct for the restrictions on ϑ that are ignored in the first term. According to (A.7), the angles $\vartheta_0(M^2, \vec{l}_\perp'^2)$ and $\vartheta_1(M^2, \vec{l}_\perp'^2)$ in (A.9) are obtained from

$$\cos \vartheta_{0,1}(M^2, \vec{l}_\perp'^2) = \frac{m_{0,1}^2 - M^2 - \vec{l}_\perp'^2}{2M\sqrt{\vec{l}_\perp'^2}}, \quad (\text{A.11})$$

where m_1^2 stands for $m_1^2 \equiv m_1^2(W^2)$.

For a sufficiently restricted range of the integrations over $d\vec{l}_\perp'^2$ in (A.3) and (A.4), the M'^2 correction term, the third term on the right-hand side in (A.9), vanishes in the limit of $m_1^2(W^2) \rightarrow \infty$. More specifically, for the ansatz (2.3), or equivalently,

$$\bar{\sigma}_{(q\bar{q})_L^{J=1p}}(\vec{l}_\perp'^2, W^2) = \bar{\sigma}_{(q\bar{q})_T^{J=1p}}(\vec{l}_\perp'^2, W^2) = \frac{\sigma^{(\infty)}(W^2)}{\pi} \delta(\vec{l}_\perp'^2 - \Lambda_{sat}^2(W^2)), \quad (\text{A.12})$$

upon ignoring the second term on the right-hand side in (A.9) for $\mu(W^2) = m_0^2/\Lambda_{sat}^2(W^2) \ll 1$, and for $m_1^2(W^2) \rightarrow \infty$, one obtains [6, 7] the photoabsorption cross sections described in (2.7) to (2.17) of the main text. Neglecting the second term on the right-hand side in (A.9), the m_0^2 -correction term, will be justified in Appendix C.

In what follows, we consider the effect of the finite bound $m_1^2(W^2)$, according to (A.9) and (A.10), on the cross sections (A.3) and (A.4) upon substitution of (A.12).

The contribution to the photoabsorption cross sections (A.3) and (A.4) corresponding to the first term on the right-hand side in (A.9), the dominant contributions, can be fully evaluated analytically,

$$\sigma_{\gamma_L^* p}^{dom}(W^2, Q^2) = A(W^2) I_L(\Lambda_{sat}^2(W^2), Q^2, M^2) \Big|_{m_0^2}^{m_1^2(W^2)}, \quad (\text{A.13})$$

and

$$\sigma_{\gamma_T^* p}^{dom}(W^2, Q^2) = A(W^2) I_T(\Lambda_{sat}^2(W^2), Q^2, M^2) \Big|_{m_0^2}^{m_1^2(W^2)}, \quad (\text{A.14})$$

where by definition

$$A(W^2) = \frac{\alpha R_{e^+e^-}}{3\pi} \sigma^{(\infty)}(W^2), \quad (\text{A.15})$$

and

$$I_L(\Lambda_{sat}^2(W^2), Q^2, M^2) = \frac{-Q^2}{Q^2 + M^2} + Q^2 L_1(\Lambda^2, Q^2, M^2), \quad (\text{A.16})$$

as well as

$$\begin{aligned} I_T(\Lambda_{sat}^2(W^2), Q^2, M^2) &= -\frac{\Lambda^2}{2} L_1(\Lambda^2, Q^2, M^2) - I_L(\Lambda^2, Q^2, M^2) \\ &+ \frac{1}{2} \ln \frac{Q^2 + M^2}{\sqrt{X(\Lambda^2, Q^2, M^2)} + Q^2 + M^2 - \Lambda^2}. \end{aligned} \quad (\text{A.17})$$

In (A.16) and (A.17),

$$\begin{aligned} X(\Lambda^2, Q^2, M^2) &= (M^2 - \Lambda^2 + Q^2)^2 + 4Q^2\Lambda^2, \\ L_1(\Lambda^2, Q^2, M^2) &= \frac{1}{\sqrt{\Lambda^2(\Lambda^2 + 4Q^2)}} \\ &\times \ln \frac{\sqrt{\Lambda^2(\Lambda^2 + 4Q^2)} \sqrt{X(\Lambda^2, Q^2, M^2)} + \Lambda^2(3Q^2 - M^2 + \Lambda^2)}{Q^2 + M^2} \end{aligned} \quad (\text{A.18})$$

and Λ^2 stands for $\Lambda^2 \equiv \Lambda_{sat}^2(W^2)$ on the right-hand sides in (A.16) to (A.18).

We turn to the correction terms, the second and the third term on the right-hand side in (A.9). Upon integrating over $d\vartheta$, one obtains

$$\begin{aligned} \Delta\sigma_{\gamma_{Lp}^*}^{(m_0^2)}(W^2, Q^2) &= -A(W^2) \int_{(\Lambda-m_0)^2}^{(\Lambda+m_0)^2} dM^2 \\ &\times \left[\frac{Q^2}{(Q^2 + M^2)^2} \frac{\pi - \theta_0(\Lambda^2, M^2)}{\pi} \right. \\ &\quad \left. - \frac{Q^2}{(Q^2 + M^2)\sqrt{X(\Lambda^2, Q^2, M^2)}} \left(1 - \frac{2}{\pi} \arctan \sqrt{Y_0(\Lambda^2, Q^2, M^2)}\right) \right], \quad (\text{A.19}) \end{aligned}$$

and

$$\begin{aligned} \Delta\sigma_{\gamma_{Tp}^*}^{(m_0^2)}(W^2, Q^2) &= -A(W^2) \frac{1}{2} \int_{(\Lambda-m_0)^2}^{(\Lambda+m_0)^2} dM^2 \\ &\times \left[\frac{M^2 - Q^2}{(Q^2 + M^2)^2} \frac{\pi - \theta_0(\Lambda^2, M^2)}{\pi} \right. \\ &\quad \left. - \frac{M^2 - Q^2 - \Lambda^2}{(Q^2 + M^2)\sqrt{X(\Lambda^2, Q^2, M^2)}} \left(1 - \frac{2}{\pi} \arctan \sqrt{Y_0(\Lambda^2, Q^2, M^2)}\right) \right], \quad (\text{A.20}) \end{aligned}$$

as well as

$$\begin{aligned} \Delta\sigma_{\gamma_{Lp}^*}^{(m_1^2)}(W^2, Q^2) &= -A(W^2) \int_{(m_1-\Lambda)^2}^{m_1^2} dM^2 \\ &\times \left[\frac{Q^2}{(Q^2 + M^2)^2} \frac{\theta_1(\Lambda^2, M^2)}{\pi} - \frac{Q^2}{(Q^2 + M^2)\sqrt{X(\Lambda^2, Q^2, M^2)}} \frac{2}{\pi} \arctan \sqrt{Y_1(\Lambda^2, Q^2, M^2)} \right], \quad (\text{A.21}) \end{aligned}$$

and

$$\begin{aligned} \Delta\sigma_{\gamma_{Tp}^*}^{(m_1^2)}(W^2, Q^2) &= -A(W^2) \frac{1}{2} \int_{(m_1-\Lambda)^2}^{m_1^2} dM^2 \\ &\times \left[\frac{M^2 - Q^2}{(Q^2 + M^2)^2} \frac{\theta_1(\Lambda^2, M^2)}{\pi} - \frac{M^2 - Q^2 - \Lambda^2}{(Q^2 + M^2)\sqrt{X(\Lambda^2, Q^2, M^2)}} \frac{2}{\pi} \arctan \sqrt{Y_1(\Lambda^2, Q^2, M^2)} \right], \quad (\text{A.22}) \end{aligned}$$

where $\theta_j(\Lambda^2, M^2)$ and $Y_j(\Lambda^2, Q^2, M^2)$ are given by

$$\theta_j(\Lambda^2, M^2) = \arccos\left(\frac{m_j^2 - M^2 - \Lambda^2}{2\sqrt{M^2\Lambda^2}}\right), \quad (0 \leq \theta_j \leq \pi), \quad (\text{A.23})$$

and

$$Y_j(\Lambda^2, Q^2, M^2) = \frac{Q^2 + (M - \Lambda)^2}{Q^2 + (M + \Lambda)^2} \times \frac{1 - \cos \theta_j(\Lambda^2, M^2)}{1 + \cos \theta_j(\Lambda^2, M^2)}, \quad (\text{A.24})$$

where $j = 0, 1$.

The dependence of $\theta_j(\Lambda^2, M^2)$ and $Y_j(\Lambda^2, Q^2, M^2)$ on the integration variable M^2 requires numerical integration of the correction terms (A.19) to (A.22).¹³ The correction terms (A.19) and (A.20) will be analysed in Appendix C.

A considerable simplification of the various contributions to the cross sections in (A.13) and (A.14), as well as in (A.21) and (A.22), is obtained by a restriction to realistic values of the parameters $m_0^2, m_1^2(W^2) = \xi \Lambda_{sat}^2(W^2)$ and $\Lambda_{sat}^2(W^2)$. Expansion in terms of

$$\mu(W^2) = \frac{m_0^2}{\Lambda_{sat}^2(W^2)} \ll 1 \quad (\text{A.25})$$

and

$$\frac{1}{\xi} \ll 1 \quad (\text{A.26})$$

will then lead to the photoabsorption cross sections in (2.34) of the main text.

We proceed in two steps. In a first step, we analyse the cross sections in the color-transparency limit of $\eta(W^2, Q^2) \gg 1$. Taking into account the leading terms in the expansion in $\mu(W^2), 1/\xi$ and $1/\eta(W^2, Q^2)$, the cross sections for the dominant terms in (A.13) and (A.14) take the simple form

$$\sigma_{\gamma_{Lp}^*}^{dom}(W^2, Q^2) = A(W^2) \frac{1}{6\eta} \frac{u^3 + 3u^2 + 6u}{(1+u)^3} \quad (\text{A.27})$$

and

$$\sigma_{\gamma_{Tp}^*}^{dom}(W^2, Q^2) = A(W^2) \frac{1}{3\eta} \frac{2u^3 + 6u^2}{2(1+u)^3}, \quad (\text{A.28})$$

where u denotes the ratio

$$u \equiv u(\eta(W^2, Q^2)) = \frac{\xi}{\eta(W^2, Q^2)} = \frac{m_1^2(W^2)}{Q^2 + m_0^2}. \quad (\text{A.29})$$

The $m_1^2(W^2)$ correction terms, given by the integrals (A.21) and (A.22), are treated as follows. We replace the integration variable M^2 by $0 \leq x' \leq 1$, according to

$$\begin{aligned} M^2 &= (2m_1\Lambda - \Lambda^2)x' + (m_1 - \Lambda)^2 \\ &= \xi\Lambda^2 \left(1 - \frac{2}{\sqrt{\xi}}(1 - x') + \frac{1}{\xi}(1 - x') \right), \end{aligned} \quad (\text{A.30})$$

¹³A computer program for the evaluation of the photoabsorption cross section according to (A.13), (A.14) and (A.19) to (A.22) is available.

and expand the integrands in powers of the small parameters $1/\xi$, $\mu(W^2)$ and $1/\eta(W^2, Q^2)$. A somewhat lengthy analysis, upon carrying out the integration over dx' , yields the $m_1^2(W^2)$ correction terms,

$$\Delta\sigma_{\gamma_{Lp}^*}^{(m_1^2)}(W^2, Q^2) = -A(W^2)\frac{1}{6\eta}\frac{6u}{(1+u)^3}, \quad (\text{A.31})$$

and

$$\Delta\sigma_{\gamma_{Tp}^*}^{(m_1^2)}(W^2, Q^2) = -A(W^2)\frac{1}{3\eta}\frac{3u^2 - 3u}{2(1+u)^3}. \quad (\text{A.32})$$

Addition of (A.27) and (A.31), as well as addition of (A.28) and (A.32), yields

$$\sigma_{\gamma_{Lp}^*}(W^2, Q^2) = A(W^2)\frac{1}{6\eta}G_L(u), \quad (\text{A.33})$$

and

$$\sigma_{\gamma_{Tp}^*}(W^2, Q^2) = A(W^2)\frac{1}{3\eta}G_T(u), \quad (\text{A.34})$$

where [9]

$$G_L(u) = \frac{2u^3 + 6u^2}{2(1+u)^3}, \quad (\text{A.35})$$

and

$$G_T(u) = \frac{2u^3 + 3u^2 + 3u}{2(1+u)^3}. \quad (\text{A.36})$$

compare (2.35) in the main text.

So far we analysed the cross sections (A.3) and (A.4) for $\eta(W^2, Q^2) \gg 1$. The dependence of the cross sections on the upper limit $m_1^2(W^2)$ for $\eta(W^2, Q^2) > 1$ turned out to be given by the correction factors (A.35) and (A.36) that depend on the ratio $u(\eta(W^2, Q^2)) = \xi/\eta(W^2, Q^2)$ in (A.29). With the assumption that the dependence on $m_1^2(W^2)$ also for $\eta(W^2, Q^2) < 1$ is determined by a correction factor that is an analytic function of this ratio $u(\eta(W^2, Q^2)) = \xi/\eta(W^2, Q^2)$, the correction factors in the extension of the cross sections (A.33) and (A.34) to values of $\eta(W^2, Q^2) < 1$ have to coincide with $G_L(u)$ and $G_T(u)$ in (A.35) and (A.36). In (A.33) and (A.34), accordingly, we have to perform the replacements

$$\begin{aligned} \frac{1}{6\eta} &\rightarrow I_L^{(1)}(\eta, \mu), \\ \frac{1}{3\eta} &\rightarrow I_T^{(1)}(\eta, \mu), \end{aligned} \quad (\text{A.37})$$

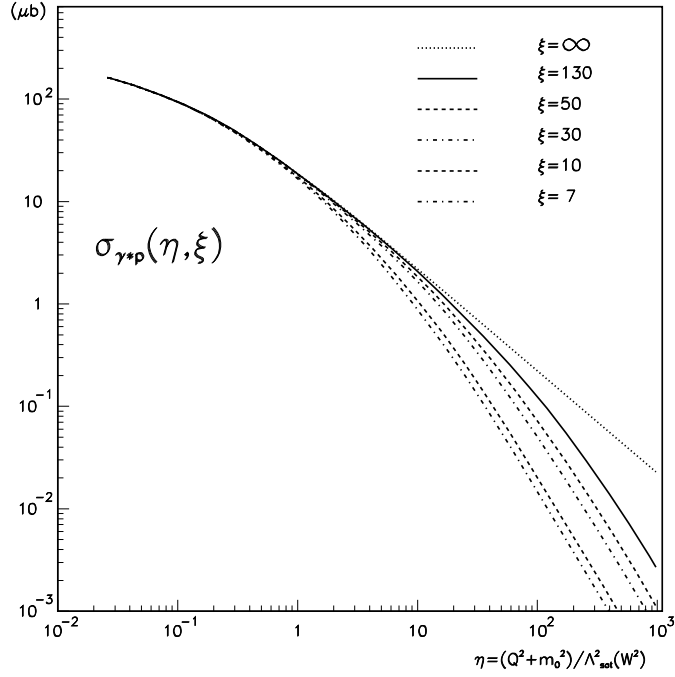


Figure A.1: The effect on the total photoabsorption cross section of the exclusion of high-mass $q\bar{q}$ fluctuations via $M_{q\bar{q}}^2 \leq \xi \Lambda_{sat}^2(W^2)$.

leading to

$$\begin{aligned}\sigma_{\gamma_L^* p}(W^2, Q^2) &= A(W^2) I_L^{(1)}(\eta, \mu) G_L(u), \\ \sigma_{\gamma_T^* p}(W^2, Q^2) &= A(W^2) I_T^{(1)}(\eta, \mu) G_T(u),\end{aligned}\tag{A.38}$$

where the general $m_1^2 \rightarrow \infty$ expression for $I_L^{(1)}(\eta, \mu)$ and $I_T^{(1)}(\eta, \mu)$ are given by (2.9) or (2.14) in the main text. The result (A.38), upon inserting the definition (A.15) for $A(W^2)$, yields (2.34) (for $\rho = 1$) in the main text.

In fig. A1, we illustrate the dependence of $\sigma_{\gamma^* p}(W^2, Q^2) = \sigma_{\gamma^* p}(\eta(W^2, Q^2), \xi)$ on the parameter ξ introduced in (2.30) via $M_{q\bar{q}}^2 \leq m_1^2(W^2) = \xi \Lambda_{sat}^2(W^2)$. For $\eta(W^2, Q^2) \lesssim 1$, high-mass fluctuations of the photon, $\gamma^* \rightarrow q\bar{q}$, do not contribute, and the limit of $\xi \rightarrow \infty$ becomes valid.

We turn to the transverse-size-enhancement factor ρ introduced in (2.24) and (2.33). Quark-antiquark ($q\bar{q}$) states of given mass $M_{q\bar{q}}$ originating from longitudinally and trans-

versely polarized photons, $\gamma_L^* \rightarrow (q\bar{q})_L$ and $\gamma_T^* \rightarrow (q\bar{q})_T$, differ in their internal transverse momentum distributions. The normalized $z(1-z)$ distributions [15], [9]

$$f_L(z(1-z)) = 6z(1-z) \quad (\text{A.39})$$

and

$$f_T(z(1-z)) = \frac{3}{2}(1-2z(1-z)) \quad (\text{A.40})$$

imply different average transverse momenta of the quarks originating from $\gamma_L^* \rightarrow (q\bar{q})_L$ and $\gamma_T^* \rightarrow (q\bar{q})_T$ transitions. Passing from the ratio of the average internal transverse momenta squared of the quarks (antiquarks) in the $(q\bar{q})_L^{J=1}$ and $(q\bar{q})_T^{J=1}$ states to the ratio of the transverse sizes of the $(q\bar{q})_L^{J=1}$ and $(q\bar{q})_T^{J=1}$ states, from (A.39) and (A.40), by invoking the uncertainty principle, one finds an enhancement in the average transverse size of magnitude [15], [9]

$$\rho = \frac{4}{3} \quad (\text{A.41})$$

of the $(q\bar{q})_T^{J=1}$ relative to the $(q\bar{q})_L^{J=1}$ state. The average transverse size of $q\bar{q}$ fluctuations being unaffected by the Lorentz-boost transformation supplying the γ^*p interaction energy W , the ratio ρ quite generally, i.e. independently of the specific value of $\rho = 4/3$ in (A.41), must be a W -independent constant, $\rho = \text{const.}$

The color-gauge-invariant interaction (2.2) in terms of $(q\bar{q})_{L,T}^{J=1}$ states, in the appropriate high-energy limit of $\vec{l}_\perp'^2 \vec{r}_\perp'^2 \ll 1$ implies vanishing of the dipole cross section in the limit of vanishing dipole size, or proportionality to $\vec{r}_\perp'^2$ [9],

$$\bar{\sigma}_{(q\bar{q})_{L,T}^{J=1}p}(\vec{r}_\perp'^2, W^2) = \frac{1}{4}\pi\vec{r}_\perp'^2 \int d\vec{l}_\perp'^2 \vec{l}_\perp'^2 \bar{\sigma}_{(q\bar{q})_{L,T}^{J=1}p}(\vec{l}_\perp'^2, W^2). \quad (\text{A.42})$$

The factor multiplying $\vec{r}_\perp'^2$ on the right-hand side in (A.42), for the dipole cross section of the ansatz (2.3), or equivalently according to the ansatz (A.12), is proportional to $\Lambda_{sat}^2(W^2)$. A transverse-size enhancement of magnitude ρ , corresponding to an enhancement of the dipole cross section for $(q\bar{q})_T^{J=1}$ states, accordingly implies the replacement

$$\Lambda_{sat}^2(W^2) \rightarrow \rho\Lambda_{sat}^2(W^2) \quad (\text{A.43})$$

to be carried out in (A.12), modifying (A.12) to become

$$\begin{aligned} \bar{\sigma}_{(q\bar{q})_L^{J=1}p}(\vec{l}_\perp'^2, W^2) &= \frac{\sigma^{(\infty)}(W^2)}{\pi} \delta(\vec{l}_\perp'^2 - \Lambda_{sat}^2(W^2)), \\ \bar{\sigma}_{(q\bar{q})_T^{J=1}p}(\vec{l}_\perp'^2, W^2) &= \frac{\sigma^{(\infty)}(W^2)}{\pi} \delta(\vec{l}_\perp'^2 - \rho\Lambda_{sat}^2(W^2)). \end{aligned} \quad (\text{A.44})$$

Inserting (A.44) into (A.42) yields (2.42) and (2.41) in the main text.

Returning to the photoabsorption cross sections in (A.38), we apply the substitution (A.43) to the transverse cross section via

$$I_T^{(1)}(\eta, \mu) \rightarrow I_T^{(1)}\left(\frac{\eta}{\rho}, \frac{\mu}{\rho}\right) \quad (\text{A.45})$$

yielding (2.33) and (2.34) in the main text.¹⁴

The introduction of the transverse-size-enhancement factor ρ according to (A.39) to (A.41), leading to (A.44), makes use of the dipole cross sections for longitudinally and transversely polarized dipole states, $(q\bar{q})_L^{J=1}$ and $(q\bar{q})_T^{J=1}$ in (A.12). In ref. [9], we introduced an ansatz for the dipole cross section $\sigma_{(q\bar{q})}(\vec{r}_\perp, z(1-z), W^2)$ in (2.1) that replaces the ansatz (A.12), and equivalently (2.4), and contains the cases of $\rho = 1$, as well as $\rho \neq 1$, and specifically $\rho = 4/3$ from (A.41). The factor ρ depends on a free parameter, $\rho = \rho(\epsilon \equiv 1/6a)$. Explicitly,

$$\rho(\epsilon) = \frac{1}{2\sqrt{1-4\epsilon}} \left(\ln \frac{(1 + \sqrt{1-4\epsilon})^2}{4\epsilon} - \sqrt{1-4\epsilon} \right) \cong \frac{1}{2} \ln \frac{1}{\epsilon}. \quad (\text{A.46})$$

The photoabsorption cross sections (2.34) to (2.36) of the present paper form an accurate closed approximate form of the results in ref. [9]. The results of ref. [9] explicitly demonstrate the consistency of the photoabsorption cross sections in (2.34) to (2.36) with the general form of the CDP as formulated in (2.1) with (2.2).

Appendix B. The Mass Dispersion Relation of Generalized Vector Dominance

In this Appendix, we explicitly demonstrate the connection between the CDP and the mass dispersion relation of the generalized vector dominance (GVD) approach [1] of the 1970's. We consider the total photoabsorption cross section given by the sum of the longitudinal and transverse cross sections in (A.3) and (A.4). We restrict ourselves to the case of helicity independence of the $q\bar{q}$ -proton interaction,

$$\bar{\sigma}_{(q\bar{q})_L^{J=1p}}(\vec{l}_\perp'^2, W^2) = \bar{\sigma}_{(q\bar{q})_T^{J=1p}}(\vec{l}_\perp'^2, W^2) \equiv \bar{\sigma}_{(q\bar{q})^{J=1p}}(\vec{l}_\perp'^2, W^2) \quad (\text{B.1})$$

¹⁴One may alternatively be led to the conclusion that also $G_T(u) \rightarrow G_T(u = \xi/\eta \rightarrow \rho\xi/\eta)$ in (A.36). Effectively this would amount to a different value of the parameter ξ in the transverse case relative to the longitudinal one. The replacement (A.45) is identical to the approach of ref. [9], see next paragraph.

that is realized by the ansatz (2.3). Summation of (A.3) and (A.4) yields

$$\begin{aligned} \sigma_{\gamma^*p}(W^2, Q^2) &= \sigma_{\gamma_{Lp}^*}(W^2, Q^2) + \sigma_{\gamma_{Tp}^*}(W^2, Q^2) = \frac{\alpha R_{e^+e^-}}{6\pi} \\ &\times \int dM^2 \int dM'^2 \int d\vec{l}_\perp'^2 \bar{\sigma}_{(q\bar{q})^{J=1p}}(\vec{l}_\perp'^2, W^2) \frac{w(M^2, M'^2, \vec{l}_\perp'^2)(M'^2 - M^2 + \vec{l}_\perp'^2)}{(Q^2 + M^2)(Q^2 + M'^2)}. \end{aligned} \quad (\text{B.2})$$

Substituting the $J = 1$ projections of the ansatz (2.3),

$$\begin{aligned} \bar{\sigma}_{(q\bar{q})_L^{J=1p}}(\vec{l}_\perp'^2, W^2) &= \bar{\sigma}_{(q\bar{q})_T^{J=1p}}(\vec{l}_\perp'^2, W^2) = \\ &= \frac{\sigma^{(\infty)}(W^2)}{\pi} \delta(\vec{l}_\perp'^2 - \Lambda_{sat}^2(W^2)), \end{aligned} \quad (\text{B.3})$$

(B.2) becomes

$$\begin{aligned} \sigma_{\gamma^*p}(W^2, Q^2) &= \frac{\alpha R_{e^+e^-}}{6\pi^2} \sigma^{(\infty)}(W^2) \\ &\times \int dM^2 \int dM'^2 \frac{w(M^2, M'^2, \Lambda_{sat}^2(W^2))(M'^2 - M^2 + \Lambda_{sat}^2(W^2))}{(Q^2 + M^2)(Q^2 + M'^2)}. \end{aligned} \quad (\text{B.4})$$

The right-hand sides in (B.2) and (B.4) are identical in their structures to the mass-dispersion relation of the GVD approach of the 1970's [1], [2]. In the 1970's, the mass dispersion relation was postulated by extrapolating the role of the low-lying vector mesons ρ^0, ω and ϕ in e^+e^- annihilation and (diffractive) photoproduction to a conjectured continuum of high-mass-vector-state contributions predicted to be observed in e^+e^- annihilation experiments at sufficiently high energies. The approach in ref. [1] is based on the simplifying assumption of the ‘‘diagonal approximation’’, $M^2 = M'^2$ in (B.4). The destructive interference of the QCD gauge theory contained in (2.2), in ref. [2] was anticipated by introducing off-diagonal, $M^2 \neq M'^2$, transitions, compare (B.4).

Appendix C. The m_0^2 correction in (2.8) and (A.9).

We discuss the (relative) magnitude of the m_0^2 -dependent corrections, $\Delta\sigma_{\gamma_{L,Tp}^*}^{(m_0^2)}(W^2, Q^2)$, to the total photoabsorption cross section, $\sigma_{\gamma_{L,Tp}^*}(W^2, Q^2)$ in (2.7) with (2.8), as introduced according to (A.9) and specified in (A.19) and (A.20). From the restricted range of the integrations in (A.19) and (A.20), we expect contributions of order $\mu(W^2) = m_0^2/\Lambda_{sat}^2(W^2) \ll 1$.

Rewriting $\Delta\sigma_{\gamma_{L,T}^*}^{(m_0^2)}(W^2, Q^2)$ from (A.19) and (A.20) as

$$\Delta\sigma_{\gamma_{L,T}^*}^{(m_0^2)}(W^2, Q^2) = A(W^2)I_{L,T}^{(1)}(\eta, \mu)\delta_{L,T}^{(m_0^2)}(\eta, \mu), \quad (\text{C.1})$$

with $\eta \equiv \eta(W^2, Q^2)$ and $\mu \equiv \mu(W^2)$, and with $A(W^2)$ from (A.15) and $I_{L,T}^{(1)}(\eta, \mu)$ from (2.9), and introducing the $Q^2 = 0$ photoproduction limit, $\sigma_{\gamma p}(W^2)$, according to (2.37), the total photoabsorption cross section becomes

$$\begin{aligned} \sigma_{\gamma^*p}(W^2, Q^2) &= \frac{\sigma_{\gamma p}(W^2)}{I_T^{(1)}(\mu, \mu)(1 + \delta_T^{(m_0^2)}(\mu, \mu))} \\ &\times \left(I_T^{(1)}(\eta, \mu)(1 + \delta_T^{(m_0^2)}(\eta, \mu)) + I_L^{(1)}(\eta, \mu)(1 + \delta_L^{(m_0^2)}(\eta, \mu)) \right). \end{aligned} \quad (\text{C.2})$$

It may be rewritten as

$$\begin{aligned} \sigma_{\gamma^*p}(W^2, Q^2) &= \frac{\sigma_{\gamma p}(W^2)}{\ln \frac{1}{\mu}} \left(I_T^{(1)}(\eta, \mu) + I_L^{(1)}(\eta, \mu) \right) \\ &\times \frac{1}{1 + \delta_T^{(m_0^2)}(\mu, \mu)} \left(1 + \frac{I_T^{(1)}(\eta, \mu)\delta_T^{(m_0^2)}(\eta, \mu) + I_L^{(1)}(\eta, \mu)\delta_L^{(m_0^2)}(\eta, \mu)}{I_T^{(1)}(\eta, \mu) + I_L^{(1)}(\eta, \mu)} \right). \end{aligned} \quad (\text{C.3})$$

The (dominant) contribution to $\sigma_{\gamma^*p}(W^2, Q^2)$, on the right-hand side of the first line in (C.3), is corrected by the m_0^2 -correction term shown in the second line of (C.3).

In the transition from (C.2) to (C.3), we used $I_T^{(1)}(\mu, \mu) = \ln(1/\mu)$ from (2.10). Upon specification of (A.20) to $Q^2 = 0$, one finds that $\delta_T^{(m_0^2)}(\mu, \mu)$ in (C.1) is approximately given by

$$\delta_T^{(m_0^2)}(\mu, \mu) \cong -\frac{\mu}{\ln \frac{1}{\mu}} < 0. \quad (\text{C.4})$$

In Table C.1, we compare the approximation (C.4) with the numerical evaluation of $\delta_T^{(m_0^2)}(\mu, \mu)$ for several values of W^2 and $m_0^2 = 0.15 \text{ GeV}^2$. The error of the approximation (C.4) decreases from about 9 % to about 1 % in the energy range considered in Table C.1.

The m_0^2 correction term in the bracket on the right-hand side in (C.3),

$$\delta^{(m_0^2)}(\eta, \mu) \equiv \frac{I_T^{(1)}(\eta, \mu)\delta_T^{(m_0^2)}(\eta, \mu) + I_L^{(1)}(\eta, \mu)\delta_L^{(m_0^2)}(\eta, \mu)}{I_T^{(1)}(\eta, \mu) + I_L^{(1)}(\eta, \mu)}, \quad (\text{C.5})$$

as well as $\delta_T^{(m_0^2)}(\mu, \mu)$, must be evaluated by numerical integrations in (A.19) and (A.20). In Table C.2, we present the numerical results for $\sigma_{\gamma^*p}(W^2, Q^2)$ in (C.3) by discriminating

$W^2(\text{GeV}^2)$	$\delta_T^{(m_0^2)}(\mu, \mu)$	$-\frac{\mu}{\ln \frac{1}{\mu}}$
50	-1.03×10^{-1}	-9.44×10^{-2}
100	-7.60×10^{-2}	-7.09×10^{-2}
625	-3.59×10^{-2}	-3.45×10^{-2}
1×10^4	-1.27×10^{-2}	-1.25×10^{-2}
4×10^4	-7.79×10^{-3}	-7.72×10^{-3}

Table C.1: Comparison of the numerical results for $\delta_T^{(m_0^2)}(\mu, \mu)$ from (A.20) and (C.1) with the analytical approximation (C.4).

between the dominant contribution based on evaluating (2.9) with (2.10), and the correction term in the second line in (C.3). To be definite, for $\sigma_{\gamma p}(W^2)$ in (C.3), for the results in Table C.2 we used the PDG fit from (2.38), and the parameters specified in (3.10) and (3.11),

$$\begin{aligned}
C_1 &= 0.31, \\
C_2 &= 0.27, \\
m_0^2 &= 0.15 \text{GeV}^2, \\
\xi &= 130.
\end{aligned} \tag{C.6}$$

The fairly small numerical values of the correction factor in Table C.2 are partially due to a cancellation between the contributions of $\delta_T^{(m_0^2)}(\eta, \mu)$ and $\delta_L^{(m_0^2)}(\eta, \mu)$ in (C.5). The corrections $\delta_T^{(m_0^2)}(\eta, \mu)$ and $\delta_L^{(m_0^2)}(\eta, \mu)$ are of opposite sign. The effect on the ratio

$$\begin{aligned}
R(W^2, Q^2) &= \frac{\sigma_{\gamma_L^* p}(W^2, Q^2)}{\sigma_{\gamma_T^* p}(W^2, Q^2)} = \frac{I_L^{(1)}(\eta, \mu)(1 + \delta_L^{(m_0^2)}(\eta, \mu))}{I_T^{(1)}(\eta, \mu)(1 + \delta_T^{(m_0^2)}(\eta, \mu))} \\
&\equiv R^{(dom)}(W^2, Q^2) \frac{1 + \delta_L^{(m_0^2)}(\eta, \mu)}{1 + \delta_T^{(m_0^2)}(\eta, \mu)}
\end{aligned} \tag{C.7}$$

is more significant, accordingly.

In Table C.3, we show a few values of $R(W^2, Q^2)$ without the m_0^2 -correction term, $R^{(dom)}(W^2, Q^2)$, and with the m_0^2 correction according to (C.7). Table C.3 shows the expected convergence to $R(W^2, Q^2) = 1/2$ according to (2.23).

In summary, the analysis of this Appendix shows that the m_0^2 -correction terms appearing in (A.9), and indicated as additional terms of $O(\mu)$ in (2.8), may be neglected in the fit to the experimental data.

$\eta(W^2, Q^2)$ $W = 225\text{GeV}$	$Q^2(\text{GeV}^2)$	$\sigma_{\gamma^*p}^{(dom)}(W^2, Q^2) (\mu\text{b})$	$\frac{1+\delta^{(m_0^2)}(\eta, \mu)}{1+\delta_T^{(m_0^2)}(\mu, \mu)}$	$\sigma_{\gamma^*p}(W^2, Q^2) (\mu\text{b})$
0.026	0	1.63×10^2	1.000	1.63×10^2
0.1	4.28×10^{-1}	9.47×10^1	1.006	9.53×10^1
1	5.63×10^0	1.90×10^1	1.007	1.92×10^1
10	5.76×10^1	2.19	1.007	2.20
100	5.77×10^2	2.23×10^{-1}	1.007	2.24×10^{-1}
1000	5.63×10^3	2.29×10^{-2}	1.007	2.31×10^{-2}

$\eta(W^2, Q^2)$ $W = 25\text{GeV}$	$Q^2(\text{GeV}^2)$	$\sigma_{\gamma^*p}^{(dom)}(W^2, Q^2) (\mu\text{b})$	$\frac{1+\delta^{(m_0^2)}(\eta, \mu)}{1+\delta_T^{(m_0^2)}(\mu, \mu)}$	$\sigma_{\gamma^*p}(W^2, Q^2) (\mu\text{b})$
0.085	0	1.19×10^2	1.000	1.19×10^2
0.1	2.63×10^{-2}	1.08×10^2	1.011	1.09×10^2
1	1.61×10^0	2.02×10^1	1.035	2.10×10^1
10	1.75×10^1	2.36	1.038	2.45

Table C.2: The results for the total photoabsorption cross section including the m_0^2 correction, showing that the m_0^2 correction in (C.3) and (C.5) can safely be neglected in the numerical fits to the experimental data for the total photoabsorption cross section.

$Q^2(\text{GeV}^2)$	$R^{(dom)}(W^2, Q^2)$	$R(W^2, Q^2)$
0.001	0.001	0.001
0.01	0.013	0.014
0.1	0.101	0.108
1.0	0.319	0.343
10	0.457	0.487
100	0.494	0.501
1000	0.499	0.500

Table C.3: The ratio $R(W^2, Q^2)$ from (C.7) for $W^2 = (200)^2 \text{ GeV}^2$.

References

- [1] J.J. Sakurai and D. Schildknecht, Phys. Lett. **B40** (1972) 121; **B41** (1972) 489; **B42** (1972) 216;
B. Gorczyca, D. Schildknecht, Phys. Lett. **B47** (1973) 71.
- [2] H. Fraas, B.J. Read and D. Schildknecht, Nucl. Phys. **B86** (1975) 346;
R. Devenish and D. Schildknecht, Phys. Rev. **D19** (1976) 93.
- [3] D. Schildknecht, Acta Physica Polonica **B37** (2006) 595, [arXiv:hep-ph/0511090].
- [4] F.E. Low, Phys. Rev. **D12** (1975) 163;
S. Nussinov, Phys. Rev. Lett. **34** (1975) 1286; Phys. Rev. **D14** (1976) 246;
J. Gunion, D. Soper, Phys. Rev. **D15** (1977) 2617.
- [5] N.N. Nikolaev, B.G. Zakharov, Z. Phys. **C49** (1991) 607.
- [6] G. Cvetic, D. Schildknecht, A. Shoshi, Eur. Phys. J **C13** (2000) 301.
- [7] D. Schildknecht, Contribution to Diffraction 2000, Cetraro, Italy, September 2-7, 2000, Nucl. Phys. B, Proc. Supplement 99 (2001) 121;
D. Schildknecht, B. Surrow, M. Tentyukov, Phys. Lett. **B499** (2001) 116;
G. Cvetic, D. Schildknecht, B. Surrow, M. Tentyukov, EPJ **C20** (2001) 77.
- [8] D. Schildknecht, Contribution to DIS 2001, The 9th International Workshop on Deep Inelastic Scattering, Bologna, Italy, 2001, G. Brassi et al. (Eds.), World Scientific, Singapore, 2002, p. 798;
D. Schildknecht, B. Surrow and M. Tentyukov, Mod. Phys. Lett. **A16** (2001) 1829.
- [9] M. Kuroda, D. Schildknecht, Phys. Rev. **D85** (2012) 094001.
- [10] D. Schildknecht, Invited Talk, Ringberg Workshop on New Trends in HERA Physics, Ringberg Castle, September 25-28, 2011, Nucl. Phys. B, Proc. Supplement **222-224** (2012) 108;
D. Schildknecht, Invited Talk, 50th International School of Subnuclear Physics, Erice, Italy, June 23 – July 2, 2012, arXiv: 1210.0733v1 [hep-ph], Subnucl. Ser. 50 (2014),

- ed. by A. Zichichi (World Scientific) and Modern Physics Letters A, Vol. 29, No. 25 (2014) 1430028;
- D. Schildknecht, AIP Conf. Proc.1523 (2012) 329, Proceedings of Diffraction 2012 (American Institute of Physics, A. Papa, editor), Lanzarote, Canary Islands (Spain), September 10-15,2012, arXiv: 1301.0714v1 [hep-ph];
- D. Schildknecht, Invited Talk, International School of Subnuclear Physics, 52nd Course, Erice - Sicily, June 24 – July 3, 2014, arXiv: 1411.0498 [hep-ph] to appear in the Proceedings, ed. by A. Zichichi (World Scientific).
- [11] M. Kuroda and D. Schildknecht, EPJ **C37** (2004) 205; Erratum ibid. **C44** (2005) 613; Phys. Lett. **B638** (2006) 473.
 - [12] M. Kuroda and D. Schildknecht, Phys. Rev. **D88** (2013) 053007.
 - [13] C. Ewerz and O. Nachtmann, Annals Phys. **322** (2007) 1635; Annals Phys. **322** (2007) 1670.
 - [14] D. Schildknecht and F. Steiner, Phys. Lett. **B56** (1975) 36.
 - [15] M. Kuroda and D. Schildknecht, Phys. Lett. **B670** (2008) 129;
D. Schildknecht, Phys. Lett. **B716** (2012) 413.
 - [16] T. Nieh, Phys. Rev. **D1** (1970) 3161; L. Stodolsky, Phys. Rev. Lett. **18** (1967) 135;
B.L. Joffe, Phys. Lett. **30 B** (1969) 123.
 - [17] C. Bilchak, D. Schildknecht, Phys. Lett. **B233** (1989) 461.
 - [18] M. Kuroda and D. Schildknecht, Phys. Rev. **D67** (2003) 094008.
 - [19] S. Donnachie and P. Landshoff, Phys. Lett. **B296** (1992) 227.
 - [20] Particle Data Group, Phys. Rev. **D86** (2012) 1.
 - [21] W. Heisenberg, Vorträge über kosmische Strahlung (Springer, Berlin, 1953), p. 155,
reprinted in W. Heisenberg, Collected Works, Series B (Springer, Berlin,1984) p.498;
Die Naturwissenschaften **61** (1974), 1, reprinted in Collected Works, Series B, p. 912.
 - [22] M. Froissart, Phys. Rev. **123** (1961) 1053.

- [23] M.M. Block, E. Berger and C.-I. Tan, Phys. Rev. Lett. **97** (2006) 252003; E. Berger, M. Block and C.-I. Tan, Phys. Rev. Lett. **98** (2007) 242001; M.M. Block, L. Durand, P. Ha and D. McKay, arXiv: 1302.6119v2 [hep-ph].
- [24] H1 and ZEUS collaborations, JHEP **1001** (2010) 109, arXiv: 0911.0884 [hep-ex] and arXiv: 1506.06042 [hep-ex].
- [25] A. Caldwell, arXiv: 0802.0769v1; arXiv: 1601.04472.
- [26] e.g. R. Devenish and A. Cooper-Sarkar, *Deep inelastic scattering*, Oxford University Press (2004).
- [27] H1 Collaboration, Eur. Phys. J. C **74** (2014) 2814; ZEUS Collaboration, Phys. Rev. **D90** (2014) 072002.
- [28] M.M. Block, L. Durand, P. Ha, D.W. McKay, Phys. Rev. **D84** (2011) 094010.